Advances in Water Resources 140 (2020) 103594

Contents lists available at ScienceDirect

Advances in Water Resources

journal homepage: www.elsevier.com/locate/advwatres

On the multiscale characterization of effective hydraulic conductivity in random heterogeneous media: A historical survey and some new perspectives

Iván Colecchio[a], Alejandro Boschan[a], Alejandro D. Otero[a,b], Benoît Noetinger[c,*]

[a] Facultad de Ingeniería, Universidad de Buenos Aires, Paseo Colón 850, Buenos Aires, Argentina
[b] Centro de Simulación Computacional, CSC - CONICET, Godoy Cruz 2390, Buenos Aires, Argentina
[c] IFP Energies Nouvelles 1 & 4, avenue de Bois-Préau, Rueil-Malmaison Cedex 92852 France

ARTICLE INFO

Keywords:
Heterogeneous aquifers
Stochastic approach
Volume averaging
Upscaling

ABSTRACT

In large scale heterogeneous aquifer simulations, determining the appropriate coarsening scale λ to define an effective hydraulic conductivity K_{eff} is a challenging task, that involves a trade-off between accuracy and cost. Efficiently adjusting the scale λ is then key, in particular for uncertainty quantification. In this paper, we obtain improved analytical results for the variance of K_{eff}, valid at any scale, in the context of energy dissipation formulation. Using this formulation, we then derive an efficient K_{eff} numerical estimator, and compare it with those of the potential-flow average and permeameter formulations in 2D, for lognormal and binary media, over a wide range of λ and of heterogeneity. We analyze the probability density function (pdf), mean, and variance, of these estimators, comparing them with the analytical results. In the lognormal case, the pdf's are rather similar for the three estimators, and remain lognormal at all scales. In the binary case, slow convergence to an asymptotic regime is observed close to the percolation threshold.

1. Introduction

Describing effective properties of heterogeneous media has important applications in many fields of engineering and science. For example, the electrical or thermal effective conductivity of mixtures, or elastic properties of composites materials have been studied since many years ago (Maxwell, 1873; Bruggeman, 1935; Landau and Lifshitz, 1960; Auriault, 1983; Willot and Jeulin, 2009; Zhou et al., 2016). In particular, determining an effective hydraulic conductivity is of major interest in a variety of disciplines related to subsurface flow, such as groundwater flow characterization (Renard and De Marsily, 1997; Matheron, 1967; Dagan, 1989; Dagan et al., 2013), Carbon Capture Utilisation and Storage (CCUS) development (Akber Hassan and Jiang, 2012; Celia et al., 2015), and oil and gas reservoir engineering (King, 1989; Durlofsky, 1991; 1992; Preux, 2016; Malinouskaya et al., 2018). The scarcity of field data (Matheron, 1967; Dagan, 1989; Hristopulos, 2020) makes it necessary to perform some sort of interpolation, with frequent use of a stochastic approach (Gelhar, 1993; Linde et al., 2015; Godoy et al., 2018) that treats the point conductivity values as a random process, eventually accompanied by field data conditioning. While the use of this approach permits a good management of uncertainty, it turns too costly to solve the flow at the fine scale provided by laboratory (micro-tomography, synchrotron), or geological sources (Dagan et al., 2013), specially for large domains.

In addition, one may want to incorporate data obtained at different support scales before interpolation. To alleviate this issues, upscaling procedures allow us to perform a mapping from a fine scale onto a coarse scale, in which the solution of the flow is less costly.

Fig. 1 shows the lengthscales and geometrical features of the upscaling process. The fine scale conductivity $k(\mathbf{r})$ ($\mathbf{r}$ is the position vector) is defined over the regional domain $\omega \subset \Re^D$, (dimension D=1, 2 or 3) at a support scale Δ. The coarsening scale λ determines a domain ϑ, over which the effective hydraulic conductivity K_{eff} is defined. One the one hand, for practical and conceptual purposes, we can establish an upper bound L for λ, determined by the largest subdomain Ω over which it is still possible to solve the flow, eventually imposing boundary conditions at $\partial\Omega$ if natural flow conditions are unknown. For example, L could be a characteristic aquifer scale. On the other hand, a lower bound for λ is given by the support scale Δ. The effective conductivity of a block or subdomain ϑ, defined by the coarsening scale λ, i.e. $K_{eff}(\lambda)$, depends on the values of $k(\mathbf{r})$ within ϑ, but also on the conditions at the boundary $\partial\vartheta$, which may be imposed or known. Moreover, $K_{eff}(\lambda)$ is a tensor in principle, however, for isotropic media, and certain flow conditions (Sánchez-Vila et al., 1995; Vereecken et al., 2007), the use of a scalar

* Corresponding author.
E-mail address: benoit.noetinger@ifpen.fr (B. Noetinger).

https://doi.org/10.1016/j.advwatres.2020.103594
Received 8 November 2019; Received in revised form 27 March 2020; Accepted 17 April 2020
Available online 29 April 2020

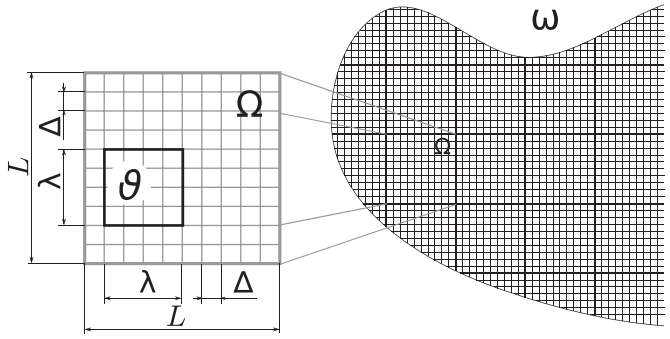

Fig. 1. Lengthscales and geometry of the upscaling procedure: The fine scale conductivity $k(\mathbf{r})$ is defined over the regional domain under investigation ω, at a support scale Δ. The upscaling procedure maps $k(\mathbf{r})$ onto $K_{eff}(\vartheta)$, while $\vartheta \subset \Omega$ is defined by the coarsening scale λ, with $\Delta < \lambda < L$.

K_{eff} is appropriate. Finding a suitable coarsening scale λ requires dealing with a trade-off between accuracy and cost: as λ increases, the cost to solve the flow decreases, but some details of the heterogeneity (and of the flow) get lost, and the values of K_{eff} become less representative of the fine description. The choice of a scale λ that retains the most salient flow features, while keeping the cost of the flow solution low, makes upscaling a challenging task.

In the following section, we revisit briefly some upscaling results, with focus on the types of media studied in most works, including the present one, i.e., lognormal and binary media, to later discuss K_{eff} distributions, and some upscaling formulations.

1.1. Previous results

Analytical methods like bounds-based approaches (Hashin and Shtrikman, 1962; Renard and De Marsily, 1997; Le Loc'H, 1987; Pozdniakov and Tsang, 2004) or power averaging (Journel et al., 1986; Desbarats and Srivastava, 1991; Masihi et al., 2016) provide a remarkable insight, although, as they estimate K_{eff} from the point values $k(\mathbf{r})$ only, they disregard the influence of the flow behavior at $\partial\Omega$.

Depending on the detailed context, homogenization techniques (Auriault, 1983; Durlofsky, 1991; Jikov et al., 2012; Armstrong et al., 2019), volume averaging techniques (Hassanizadeh and Gray, 1979; Quintard and Whitaker, 1998; Durlofsky, 1998; Whitaker, 2013; Gray and Miller, 2005; Leung and Srinivasan, 2012; Wood and Valdés-Parada, 2013; Davit and Quintard, 2017; Aguilar-Madera et al., 2019) or stochastic perturbation theory (Landau and Lifshitz, 1960; Matheron, 1967; Dagan, 1989; King, 1989; Rubin and Gómez-Hernández, 1990; Indelman and Dagan, 1993a; 1993b; Noetinger, 1994; Indelman and Abramovich, 1994; Ababou, 1994; Abramovich and Indelman, 1995; Noetinger and Gautier, 1998; Noetinger, 2000; Liao et al., 2019) were developed over many decades. All these methods provide a rigorous analytical framework supporting the existence and uniqueness of K_{eff}, for a wide variety of media types.

Analytical efforts took place mainly using perturbation theory (Gelhar, 1993; Dagan, 1989). The so called Landau-Lifschitz-Matheron (LLM) (Landau and Lifshitz, 1960; Matheron, 1967) formula reads:

$$K_{eff} :\simeq \left\langle k^{(1-\frac{2}{D})} \right\rangle^{\frac{1}{(1-\frac{2}{D})}}, \tag{1}$$

In the case of a lognormal distribution of fine scale conductivity, this formula can be written under the equivalent form (King, 1989; Noetinger, 1994):

$$\langle K_{eff} \rangle = \exp \langle \log(k) \rangle e^{(\frac{1}{2}-\frac{1}{D})C_{\log k}(\mathbf{r}=0)} = K_g e^{(\frac{1}{2}-\frac{1}{D})C_{\log k}(\mathbf{r}=0)}.$$

The notation $\langle \cdots \rangle$ indicates ensemble arithmetic averaging over all the possible realizations of the fine scale structure. K_g denotes the geometric mean of the fine grid conductivity, and $C_{\log k}(\mathbf{r}=0)$ the variance of its logarithm. In this work, wherever the expressions $\log(k)$ or $\log(K_{eff})$ are shown, it is implied that the argument of the logarithm is divided by 1 m/day, to make it dimensionless.

In most cases, an ergodicity assumption allows to replace the ensemble average by a spatial average (Ababou, 1996; Sanchez-Vila et al., 2006), such that for finite block of size L, one estimates K_{eff} as:

$$K_{eff_{block}} \simeq \left(\frac{1}{V} \int_{block} k(\mathbf{r})^{(1-\frac{2}{D})} d^D\mathbf{r} \right)^{\frac{1}{(1-\frac{2}{D})}} \tag{2}$$

This formula, with dimension $D = 1, 2, 3$ whose evaluation is straightforward, is exact in 1D for any type of media, yielding the harmonic average. In 2D, it corresponds to the geometric average that was found to be exact in 2D for lognormal media by Matheron (1967), who derived it using an elegant duality argument specific to 2 dimensions. In 3D, the formula is exact up to second order (Dagan, 1993) with respect to log-conductivity variance (using a series expansion of K_{eff} up to 4th order in powers of the log-conductivity fluctuations). But in 3D, the proposed formula was shown to be inexact at third order by several authors (Indelman and Abramovich, 1994; De Wit, 1995; Stepanyants and Teodorovich, 2003).

Moreover, higher order results were shown to be structure dependent: this prevents the existence of a local evaluation expression like Eq. (1) in 3D. However, numerical tests carried out show that LLM formula is quite robust in 3D even for large log-conductivity variances (Dagan, 1989; Romeu and Noetinger, 1995; Renard and De Marsily, 1997). Some generalization of such approaches for anisotropic cases were revisited recently by Liao et al. (2019).

From a more geological point of view, a frequent organization of the subsurface heterogeneous formations in a number of hydrofacies, that correspond to different types of rock, or sediments, having a well defined hydraulic property, such as porosity or permeability, may be observed in natural systems (Journel et al., 1986; Beucher and Renard, 2016). Each facies possesses its own characteristic features. That promoted the study of the effective conductivity of composite media. Binary or bimodal media are the simplest cases, while still retaining the complexity of percolative systems. These types of media have been extensively studied using self-consistent effective medium approaches in the electrodynamical or elasticity contexts (Maxwell, 1873; Bruggeman, 1935; Landau and Lifshitz, 1960; Auriault, 1983; Pozdniakov and Tsang, 2004).

Analytical results, based on a mixing of characteristic conductivity values and bounds (Hashin and Shtrikman, 1962; 1963), exist for this type of media (Bernabé et al., 2004); in them, connectivity is implicitly taken into account.

Other authors (Pozdniakov and Tsang, 2004; Knudby and Carrera, 2005; Guin and Ritzi, 2008; Bernabé et al., 2016) studied numerically the influence of the contrast between the high and low conductivity components k^+ and k^-. The abrupt change in K_{eff} that takes place close to the percolation transition, when the k^+ component becomes connected, poses difficulties during the upscaling procedure (Boschan and Noetinger, 2012).

Indeed, percolation theory scaling (Berkowitz and Balberg, 1993; Stauffer and Aharony, 2014; Hunt et al., 2014; Hunt and Sahimi, 2017) has been used to assess K_{eff} in this type of media, but some restrictions exist:

- This scaling is only valid for media in which the proportion of high conductivity medium is close to the percolation transition,
- Percolation transition is smeared-out by finite size effects and finite conductivity contrast values.

1.2. K_{eff} probability distributions

Due to the fact that subsurface uncertainty is frequently dealt with by using a stochastic approach, it is appropriate to treat K_{eff} as a random variable characterized by a probability distribution more than by a deterministic value.

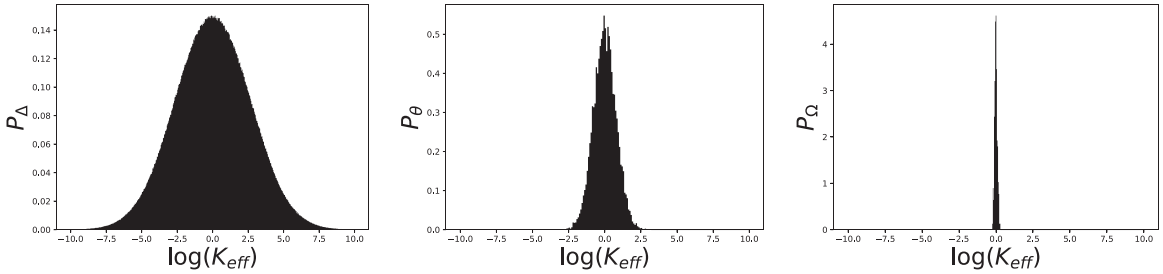

Fig. 2. Probability density function $P(K_{eff}, \lambda)$ for increasing values of the coarsening scale λ. Left: Fine scale distribution $P(k(\mathbf{r}), \Delta)$, where $k(\mathbf{r})$ follows, as an example, a lognormal distribution. Center: $P(K_{eff}, \lambda)$ becomes narrower as λ increases. Right: For $\lambda \simeq L$, $P(K_{eff}, \lambda)$ approaches a delta-like function centered on a single K_{eff} value. For dimensional reasons, the K_{eff} is normalized by a unit reference conductivity of 1 m/day.

Although the literature mainly focuses on the firsts moments of the probability density function (pdf), such as the mean and variance (Rubin and Gómez-Hernández, 1990; Sánchez-Vila et al., 1995; Sanchez-Vila et al., 2006), the shape of the pdf provides unique insight on the underlying flow situation. For example, in media samples near percolation, a bimodal pdf may yield a mean K_{eff} value that truly has a negligible occurrence probability: this situation may easily arise when dealing with fractured media or, in general, with media possessing a high degree of heterogeneity. The pdf of K_{eff} depends on the coarsening scale λ, and will be noted $P(K_{eff}, \lambda)$.

For clarity, $P(K_{eff}, \lambda)$ undergoes a transition from $P(k(\mathbf{r}), \Delta)$ to $P(K_{eff}, L)$ as λ goes from Δ to L. For $\lambda = \Delta$, the distribution of $k(\mathbf{r})$ is recovered, while for $\lambda \simeq L$, $P(K_{eff}, \lambda)$ will tend toward a delta-like distribution sharply peaked around a stable K_{eff} value (see Fig. 2). If it is possible to define a characteristic lengthscale (for example an integral scale I) for the media under consideration, a crossover is expected when λ approaches it. More conceptually, a representative elementary volume (REV) may be determined by inspecting significant changes of the shape of $P(K_{eff}, \lambda)$. The fact that the statistical sampling becomes poorer as λ increases, can be compensated, in the framework of the stochastic theory, and assuming ergodicity, by an increase in the number of ensemble realizations.

The behavior of $P(K_{eff}, \lambda)$ was addressed in several studies (King, 1989; Sanchez-Vila et al., 2006; Wen and Gómez-Hernández, 1996; Wu et al., 2013). In Boschan and Noetinger (2012), the convergence of $P(K_{eff}, \lambda)$ was studied in 3D for lognormal and binary media. In the lognormal case, $P(K_{eff}, \lambda)$ kept its lognormal nature as λ increased. If this result hold in 2D (this will be analyzed in the present work), it might stem from the work of Matheron (1967). In the binary case, it was shown that the convergence to a stable K_{eff} is slower when the k^+ component is close to the percolation transition (Stauffer and Aharony, 2014). Finally, under the ergodic hypothesis, several studies assessed the use of filtering techniques to derive $P(K_{eff}, \lambda)$ at all scales (King, 1989; Noetinger and Gautier, 1998; Noetinger, 2000; Noetinger and Zargar, 2004; Attinger, 2003; Eberhard et al., 2004).

1.3. Upscaling formulations and numerical implementations

The fact that analytical results are limited to some academic cases, and strictly valid only up to second order in 3D, imposes the use of numerical techniques to obtain K_{eff} as well as its distribution by means of Monte Carlo simulations. Several numerical techniques were developed using different approaches and provide accurate solutions (Desbarats and Srivastava, 1991; Durlofsky, 1991; Desbarats, 1992; Quintard and Whitaker, 1998; Wang et al., 2014; Zheng et al., 2017; Wang et al., 2018). The numerical implementations calculate a value K_{eff} in ϑ from the fine conductivity field $k(\mathbf{r})$, and from the boundary conditions at $\partial\vartheta$, in what constitutes a numerical solution of the closure problem posed by the associated Laplace equation. Moreover, some of them use border regions, including information of the outer neighbourhood of $\partial\vartheta$ (Wen et al., 2003). Two aspects of the solution of the closure problem by numerical simulations stand out:

1. The task of finding the optimal scale λ in each flow scenario makes upscaling a multiscale problem par excellence.
2. The choice of the formulation, in particular that of the boundary conditions, strongly affects accuracy and numerical efficiency. For example, imposing boundary conditions at $\partial\vartheta$ decouples the flow in ϑ from its outer region, in a rather invasive procedure, in view of item 1). In that sense, solving the flow in Ω once, and then employing this solution to estimate $P(K_{eff}, \lambda)$, i.e., seems less invasive and more efficient, but requires the ability to solve larger systems of equations.

From the existing upscaling formulations, the most widely used is the permeameter (Darcian) one, which, as a particularity, isolates the flow in ϑ, suffering from the drawback explained above. This formulation, and its implementation, will be formally introduced in Section 2.2. Another frequent formulation, (Rubin and Gómez-Hernández, 1990) and (Sánchez-Vila et al., 1995), uses the solution of potential and the associated flow in Ω, evaluating their averages over $\partial\vartheta$ to obtain K_{eff}. In order to obtain a scalar K_{eff}, some assumption is required.

Finally, Indelman and Dagan (1993a,b); Bøe (1994) proposed that K_{eff} could be defined by assuming that the dissipated energy is conserved during the upscaling procedure. This might be the strongest conceptual definition ever formulated, however, its implementation to obtain K_{eff} is mathematically difficult.

Aiming to reduce the computational cost, a number of approaches that combine different formulations were proposed (Chen et al., 2003; Bauer et al., 2008; Wu et al., 2013; Karimi-Fard and Durlofsky, 2016), with the support of ergodicity considerations (Ababou et al., 1989; Ababou, 1994; 1996; Desbarats and Srivastava, 1991).

1.4. Objectives

In this paper, we intend to explore analytically and numerically the multiscale nature of the upscaling procedure in the context of the different formulations in 2D. On the one hand, after reviewing the existing body of literature, we update the formulae introduced in previous studies to characterize the mean and variance of K_{eff}, valid at the scale Ω at which the boundary conditions are imposed. We derive, in the context of the energy dissipation formulation, a new expression for the variance, this time, valid at any subscale $\vartheta \subset \Omega$, up to second order in perturbation theory. On the other hand, using that formulation, we define and implement a new numerical estimator of K_{eff} based on a scalar energy dissipation average. This estimator can be obtained at any subscale λ with nearly negligible additional CPU time once the potential in Ω is solved. Aiming to provide a comprehensive view, the pdf, the mean and the variance of this estimator are compared with those of the potential-flow average estimator, and of the permeameter Darcian one, over a wide range of coarsening scales. This study is performed over

lognormal media samples with a wide range of fine grid variances, and over binary media samples spanning the percolation transition.

The paper is organized as follows: we start by presenting the overall geometry and notation, considering a steady-state Darcian flow in an heterogeneous porous medium, and perform some algebraic manipulation to express K_{eff} in terms of the viscous dissipation. We introduce then (Section 3.1) a useful variational derivation, that allows us to define K_{eff} in terms of a minimization of that dissipation. By using functional expansion techniques already developed in a previous study (Noetinger, 2013), we provide expressions for the variance of K_{eff} in Ω up to second order in the perturbation expansion (valid for small variances), later improving it, for higher variances, by using a mean-field approximation. After some more manipulation, we get in position to show how these results are valid at any subscale (i.e., the coarsening scale λ), even if the variational formulation cannot be applied at any scale smaller than Ω (the scale in which the boundary conditions are imposed). The result depends also on the covariance of $k(\mathbf{r})$, and on λ, while it is possible to apply again the mean-field technique, now at this scale, to improve it. Section 6 introduces the numerical methodology with the implementation of the three formulations, while Section 7, presents firstly a numerical validation, and then, the results regarding the multiscale dependence of K_{eff} under the different formulations.

2. Geometry, driving equations and notations

2.1. Geometry and local equations

We focus our attention on a block Ω to be upscaled in D dimensions, a square in 2D or a cube in 3D. The edges of that domain are of size L in the D directions, as sketched in Fig. 1. The potential is driven by the following Laplace equation, to be solved in the domain Ω:

$$\nabla \cdot (k(\mathbf{r})\nabla p(\mathbf{r})) = 0, \tag{3}$$

The local potential is denoted by $p(\mathbf{r})$. This equation is a combination of mass or charge conservation with a phenomenological equation relating the local flux to the local potential gradient, such as Joule, Darcy or Fourier's law that may arise after a proper averaging of the sub-scale transport processes (Hassanizadeh and Gray, 1979). In order to get a well defined problem, Dirichlet or Dirichlet-Neumann conditions must be specified at the frontier $\partial\Omega$ of the domain. These conditions will be discussed in the next section. The local conductivity, denoted by $k(\mathbf{r})$ is assumed to be scalar and to depend on position $\mathbf{r}$. The conductivity field can be discontinuous with respect to $\mathbf{r}$.

2.2. Classical Darcian definition of the effective conductivity

Here, we defer the discussion of the upscaling problem to references in Matheron (1967), Durlofsky (1991), Neuman and Orr (1993), Renard and De Marsily (1997), Quintard and Whitaker (1998), Willot and Jeulin (2009), Jikov et al. (2012). The effective conductivity can be defined using the solution of the Laplace Eq. (3), to be solved with Dirichlet boundary conditions at the inlet/outlet, denoted by P_{in} and P_{out}. Neumann no-flux boundaries are imposed on the faces of the domain parallel to the average imposed flow, which will be the x direction in the rest of the paper. This definition of K_{eff} is the so-called permeameter definition that will be sometimes denoted by K_{perm}. This corresponds physically to the basic conductivity measurement that could be performed at the laboratory, both in the Darcy or electrical context. Other boundary conditions, such as periodic (Auriault, 1983; Durlofsky, 1991; Quintard and Whitaker, 1998; Noetinger, 2013) can be chosen, but that does not change drastically the analysis, so permeameter conditions will be kept throughout the paper.

By identification with the homogeneous case, effective hydraulic conductivity is given by:

$$K_{eff} = \frac{Q}{L^{D-2}(P_{in} - P_{out})}. \tag{4}$$

Here, Q denotes the total fluid flux flowing in any section of the domain perpendicular to the mean flow x direction:

$$Q = \int_{Inlet\ face} d^{D-1}\mathbf{r}\, k(\mathbf{r})\nabla p(\mathbf{r}) \cdot \mathbf{n}. \tag{5}$$

Here, $p(\mathbf{r})$ is the unique solution of the boundary value Laplace Eq. (3) with the permeameter forcing boundary conditions.

3. Effective conductivity and viscous dissipation

For our purpose, it is useful to introduce an equivalent algebraic expression of K_{eff} that was introduced in the porous media context by Jacquard (1965), Matheron (1967), and revisited later by Wen and Gómez-Hernández (1996), Sánchez-Vila et al. (1995):

$$\begin{aligned} Q\,(P_{in} - P_{out}) &= \int_{\partial\Omega} d^{D-1}\mathbf{r}\, p(\mathbf{r})k(\mathbf{r})\nabla p(\mathbf{r}) \cdot \mathbf{n} \\ &= \int_{\Omega} d^{D}\,\mathbf{r}\, k(\mathbf{r})\,\nabla p(\mathbf{r}) \cdot \nabla p(\mathbf{r}). \end{aligned} \tag{6}$$

In order to begin with, the first equality of Eq. (6) is obtained by expressing Q in terms of integrals over the inlet and outlet faces of the domain as in Eq. (5). In the outlet, according to the convention defining positive flow opposite to the face inward normal, the expression have the opposite sign. Then, both face pressures are moved under the integral signs obtaining similar expressions. Regarding the Neumann boundary conditions on lateral faces, imposing no pressure gradient, both integrals can be combined in only one over the whole domain boundary $\partial\Omega$. Using the divergence theorem combined with Laplace Eq. (3) yields the second equality. This equation has a simple physical interpretation: The RHS corresponds to the total viscous dissipated power, that must coincide with the power spent by external forcing sources set-up to create the flow.

So, the effective conductivity may be expressed as,

$$\begin{aligned} K_{eff} &= \frac{1}{(P_{in} - P_{out})^2\, L^{D-2}} \int_{\Omega} d^{D}\mathbf{r}\, k(\mathbf{r})\,(\nabla p(\mathbf{r}))^2 \\ &= \frac{1}{\overline{\nabla p}^{2}_{\Omega,x}\, L^{D}} \int_{\Omega} d^{D}\mathbf{r}\, k(\mathbf{r})\,(\nabla p(\mathbf{r}))^2, \end{aligned} \tag{7}$$

where $\overline{\nabla p}_{\Omega,x} = -(P_{in} - P_{out})/L$ is the volume averaged gradient in the x direction (which is the mean flow direction). The average potential gradient $\overline{\nabla p}_{\Omega}$ over the block volume $|\Omega| = L^D$ is given by:

$$\overline{\nabla p}_{\Omega} = \frac{1}{|\Omega|} \int_{\Omega} d^{D}\mathbf{r}\, \nabla p(\mathbf{r}) = \frac{1}{|\Omega|} \int_{\partial\Omega} d^{(D-1)}\mathbf{r}\, p(\mathbf{r})\, \mathbf{n}. \tag{8}$$

In the case of a square or cubic Ω, the retained boundary conditions for potential p give the proposed equality in the x direction. Eq. (7) relates the effective conductivity of the whole block K_{eff} to the overall viscous dissipation and the mean forcing potential gradient norm in the imposed flow direction. It will be the starting point to define a dissipation-based effective conductivity estimator in Section 5.1.

3.1. A variational characterization of K_{eff}

We are now in position to propose an alternative formulation that proves to be useful for estimating the sensitivity of large scale parameters to variations of local conductivity. This variational characterization of K_{eff} may be formulated as follows:

$$\begin{aligned} K_{eff}\,(P_{in} - P_{out})^2\, L^{D-2} &= Q\,(P_{in} - P_{out}) \\ K_{eff}\,\overline{\nabla p}^{2}_{\Omega,x}\, L^{D} &= Min_{p(\mathbf{r})}\left\{ \Theta\{p(\mathbf{r})\} = \int_{\Omega} d^{D}\mathbf{r}\; k(\mathbf{r})\,(\nabla p(\mathbf{r}))^2 \right\}. \end{aligned} \tag{9}$$

Here, the potential fields $p(\mathbf{r})$ among which the minimization is to be performed fulfill the boundary conditions at $\partial\Omega$. The justification of Eq. (9) is classical: one has to express the extremal conditions:

$$\forall \mathbf{r},\ \frac{\delta\{\Theta\{p(\mathbf{r})\}\}}{\delta p(\mathbf{r})} = \nabla \cdot (k(\mathbf{r})\,\nabla p(\mathbf{r})) = 0.$$

The operator $\frac{\delta\{\Theta\{p(\mathbf{r})\}\}}{\delta p(\mathbf{r})}$ is a functional derivative of the functional $\Theta\{p(\mathbf{r})\}$ with respect to $p(\mathbf{r})$. A basic presentation of functional differentiation is given in Appendix A.

Using thus the particular quadratic form of $\Theta\{p(\mathbf{r})\}$, these extremal conditions give rise to Laplace Eq. (3) that governs the potential. The final result may be derived using the same methods than Eq. (6).

3.2. Functional expansion techniques for the effective conductivity

Functional techniques combined with the variational formulation are useful to derive directly second order perturbation expansion of the effective conductivity and of its associated variance. The starting point is to evaluate the sensitivity of effective conductivity with respect to local perturbations of the local conductivity, as it was derived in Noetinger (2013) and Appendix A. The starting point is to decompose the local hydraulic conductivity as:

$$k(\mathbf{r}) = \langle k\rangle + \delta k(\mathbf{r}).$$

The brackets $\langle \dots \rangle$ correspond to ensemble averaging over the conductivity realizations, to be not confused with volume averaging denoted by $\overline{\cdots}$. So $\langle \delta k(\mathbf{r})\rangle = 0$. One can use the formal equivalent of Taylor series formula, up to second order, also valid for functionals:

$$K_{eff} = \langle k\rangle + \int_\Omega d^D\mathbf{r}\ \frac{\delta K_{eff}}{\delta k(\mathbf{r})}\ \delta k(\mathbf{r}) + \frac{1}{2}\int_\Omega d^D\mathbf{r}\int_\Omega d^D\mathbf{r}'\ \frac{\delta^2 K_{eff}}{\delta k(\mathbf{r})\ \delta k(\mathbf{r}')}\ \delta k(\mathbf{r})\ \delta k(\mathbf{r}') + \dots \tag{10}$$

The reader must note that in these equations, the functional derivative must be evaluated while the nominal value of the conductivity map is a uniform value $k(\mathbf{r}) = \langle k\rangle$ (in usual function Taylor's expansions, this corresponds to the point at which the derivative is evaluated). Averaging Eq. (10) yields a second-order expansion that coincides with LLM conjecture up to this limited order. A concise derivation using functional derivatives is given in Appendix B.

4. Estimation of the variance of the effective conductivity at second order

In this section, we present expressions of the variance of the effective conductivity that are obtained in the context of second order perturbation theory. The derivations are given in Appendix C. Finally, closed expressions are given for the cases when those expressions are particularized for Gaussian covariance functions.

For the variance of the effective conductivity given by

$$C_{K_{eff}}(L) = \langle K_{eff}^2\rangle - \langle K_{eff}\rangle^2 = \langle (K_{eff} - \langle K_{eff}\rangle)^2\rangle$$

the following expression can be obtained, Eq. (C.4):

$$C_{K_{eff}}(L) = \frac{1}{|\Omega|^2}\int_\Omega d^D\mathbf{r}\, d^D\mathbf{r}'\, C_k(\mathbf{r}-\mathbf{r}'). \tag{11}$$

A mean-field approximation allows to replace each occurrence of K_{eff} and k by the corresponding logarithm, Eq. (C.7), providing the following expression that can be expected to have a more extended domain of validity for practical applications:

$$C_{\log K_{eff}}(L) = \frac{1}{|\Omega|^2}\int_\Omega d^D\mathbf{r} d^D\mathbf{r}' C_{\log k}(\mathbf{r}-\mathbf{r}'). \tag{12}$$

The resulting formula is similar to Eq. (11), replacing the covariance function by the log conductivity covariance function. For the special case of lognormal media, this is a quite natural transformation. The same can be done with the simplified formula (C.5).

In the case of the Gaussian covariance with $C_k(\mathbf{r}) = C_k(r=0)\ e^{-\frac{r^2}{2I_c^2}}$ where I_c is the correlation length, explicit analytical expressions can be derived for $C_{K_{eff}}(L)$ from Eq. (11) (see Appenidx C.2 Eq. (C.8))

$$C_{K_{eff}(L)} = C_k(r=0)\left(\frac{I_c}{L}\right)^{2D}\left[\sqrt{2\pi}\frac{L}{I_c}\ \mathrm{erf}\left(\sqrt{2}\frac{L}{I_c}\right) + 2e^{-\frac{L^2}{2I_c^2}} - 2\right]^D. \tag{13}$$

Likewise, using the simplified Eq. (C.5), one gets after integration (Eq. (C.9)):

$$C_{K_{eff}}(L) \simeq C_k(r=0)\left[\sqrt{2\pi}\frac{I_c}{L}\ \mathrm{erf}\left(2\sqrt{2}\frac{L}{I_c}\right)\right]^D. \tag{14}$$

The same calculations can be carried out for $C_{\log K_{eff}}(L)$ applying the logarithmic transformation and give analogous results using $C_{\log k}(r=0)$ and the same spatial dependence.

5. A posteriori multiscale estimators of K_{eff} distributions

In this section, two estimators providing intermediate scale effective conductivity distributions are presented. Both are computed using low-cost post processing of one up scaling closure problem at the largest available scale. These distributions will be compared to reference distributions determined by computing numerically permeameter effective conductivity of every coarse block at any scale. The resulting pdf's will be compared, as well as the associated log conductivity mean and variance. For completeness, the latter will be compared with preceding analytical results.

5.1. Dissipation estimator

5.1.1. Definition of the estimator

We consider now that the upscaling Laplace problem was solved on a single conductivity realization on the entire block Ω. The subscale effective conductivity $K_{diss}(\vartheta)$ on any given cubic (or square) sub-block of size λ included in the overall domain Ω can thus be defined as the relation between the dissipation and the average potential gradient at the block level by:

$$K_{diss}(\vartheta) = \frac{\int_\vartheta d^D\mathbf{r}\ k\,(\nabla p)^2}{\lambda^D\,\overline{\nabla p}_\vartheta^{\,2}}. \tag{15}$$

It can be observed, using Eq. (7), that if $\vartheta = \Omega$, $K_{diss}(\vartheta) = K_{eff}\times\frac{\overline{\nabla p_x}^2}{\overline{\nabla p}^2} \le K_{eff}$. In the case of statistically isotropic $k(r)$, if Ω is sufficiently large, the average potential gradient $\overline{\nabla p_y}$ perpendicular to the mean flow vanishes, so the effective conductivity determined by dissipation is equal to the usual definition: $K_{diss}(\vartheta\to\Omega) \simeq K_{eff}$.

Considering the opposite limit, $\vartheta \to 0$, it can be shown, using a Taylor expansion of the potential gradient under the integral sign, that $K_{diss}(\vartheta) = k(\mathbf{r})$ if and only if $\overline{\nabla p}^2 \simeq (\nabla p)^2 \neq 0$. This last condition corresponds to stagnation (no-flow) points. This condition is not surprising, as it can correspond to both infinite conductivity regions or to screened regions of vanishing hydraulic conductivity. In both cases, effective conductivity is not defined. Assuming that the set of these points is of vanishing measure, in most cases the original detailed conductivity map must be recovered. This criterion was already introduced and discussed by Sánchez-Vila et al. (1995) and Bauer et al. (2008). The proposed indicator fulfills two intuitive conditions for both extreme ϑ sizes. In Appendix D it is shown that the average of the dissipation estimator is in agreement with that derived for K_{eff} for volumes ϑ tending to Ω, and the structure of the finite size corrections is given too. In next Section 5.1.2, it is shown up to second order that the variance of $K_{diss}(\vartheta)$ coincides with expression (11) by replacing Ω by ϑ as integration domain. This implies that the evaluation of the variance $C_{\log K_{diss}}(\lambda)$ is obtained by replacing L by the length of the considered subscale block, λ, in Eq. (12).

5.1.2. Evaluation of the variance of block dissipation conductivity $\mathrm{K_{diss}}$

The block equivalent conductivity $K_{diss}(\vartheta)$ is given by Eq. (15), and its variance may be evaluated following the same steps that in Appendix C.

It is defined by $\langle K_{diss}(\vartheta)^2\rangle - \langle K_{diss}(\vartheta)\rangle^2 = \langle \big(K_{diss}(\vartheta) - \langle K_{diss}(\vartheta)\rangle\big)^2\rangle$. So, one gets finally:

$$\langle K_{diss}(\vartheta)^2\rangle - \langle K_{diss}(\vartheta)\rangle^2 = \int_\Omega d^D\mathbf{r}\, d^D\mathbf{r}' \frac{\delta K_{diss}(\vartheta)}{\delta k(\mathbf{r})}\frac{\delta K_{diss}(\vartheta)}{\delta k(\mathbf{r}')}\langle \delta k(\mathbf{r})\delta k(\mathbf{r}')\rangle + \dots$$

Note that at present stage, the integration volume remains the whole volume Ω, it is not restricted to ϑ because $K_{eff}(\vartheta)$ depends on the entire conductivity map that is defined on the support Ω in which the Laplace equation is solved at the beginning. We have to evaluate the functional derivative $\frac{\delta K_{diss}(\vartheta)}{\delta k(\mathbf{r})}$. The evaluation cannot be simplified because the variational principle that characterizes K_{eff} as defined in Ω is not relevant at any smaller scale. The derivative is given by:

$$\frac{\delta K_{diss}(\vartheta)}{\delta k(\mathbf{r})} = \frac{(\nabla p_0(\mathbf{r}))^2}{\lambda^D \overline{\nabla p_0}^2}\mathbf{1}_\vartheta(\mathbf{r}) + \frac{2}{\lambda^D \overline{\nabla p_0}^2}\frac{1}{\lambda^D} \left[\overline{\nabla p_0}^2 \int_\vartheta d^D\mathbf{r}' k\,\nabla p_0(\mathbf{r}')\cdot\frac{\delta \nabla p(\mathbf{r}')}{\delta k(\mathbf{r})} - \frac{1}{\lambda^D}\int_\vartheta d^D\mathbf{r}' k\,\nabla p_0(\mathbf{r}')^2 \int_\vartheta d^D\mathbf{r}''\nabla p_0(\mathbf{r}'')\cdot\frac{\delta\nabla p(\mathbf{r}'')}{\delta k(\mathbf{r})}\right].$$

In that equation, the first term involving the indicator function of ϑ denoted by $\mathbf{1}_\vartheta(\mathbf{r})$ is the remaining of the result that would be provided using the variational approach, as shown in Appendix C, Eq. (C.1). The first integral arises from the derivative of ∇p^2 under the integral sign, the second corresponds to the functional derivative of $\frac{1}{\overline{\nabla p}^2}$. Both terms are equal to 0 if $\vartheta = \Omega$. At lowest order, the spatial dependence of the conductivity k must be discarded. It appears that the second line involving twice integration vanishes because $\nabla p_0(\mathbf{r}') = \mathbf{e_x}$ is constant up to this order, so both terms cancel each other. So we obtain the same result that would be provided by the variational approach if it was applicable for block dissipation:

$$\frac{\delta K_{diss}(\vartheta)}{\delta k(\mathbf{r})} = \frac{(\nabla p_0)(\mathbf{r})^2}{\lambda^D \overline{\nabla p}^2}\mathbf{1}_\vartheta(\mathbf{r}).$$

Gathering all the preceding results, we obtain the following formula for the variance of the dissipation estimator at scale ϑ:

$$\langle (K_{diss}(\vartheta)^2 - \langle K_{diss}(\vartheta)\rangle^2\rangle = \frac{1}{|\vartheta|^2}\int_\vartheta d^D\mathbf{r} d^D\mathbf{r}' C_k(\mathbf{r}-\mathbf{r}'). \tag{16}$$

Up to second order, this formula is analogous to the variance in Eq. (C.3) of the full up scaled hydraulic conductivity K_{eff}. The corresponding formulation using logarithms is similar at this order. This result allows to extend the validity of Eqs. (11) and (12) to subscale blocks ϑ.

5.2. Block average conductivity estimator

Another K_{eff} estimator on subvolume ϑ can be introduced, defined as

$$K_{ave}(\vartheta) = \frac{\overline{Q}_x}{\lambda^{D-1}\overline{\nabla P}_x}.$$

This expression is based on Darcy equation where $\overline{Q}$ is the flow rate and $\overline{\nabla P}$ the potential gradient, both volume-averaged over domain ϑ of size λ. This estimator was studied by Rubin and Gómez-Hernández (1990), Sánchez-Vila et al. (1995), Renard and De Marsily (1997), Bauer et al. (2008). In particular, using a second order expansion, Rubin and Gómez-Hernández (1990) computed the average and variance of $\log(K_{ave}(\vartheta))$ as a function of ϑ and the input covariance function of the conductivity that correspond to the observed statistical parameters observed at scale L. They give the following expressions:

$$\langle \log K_{ave}(\vartheta)\rangle = \log K_g + \left(\frac{1}{2} - \frac{1}{D}\right)(1-\alpha)\, C_{\log k}(\mathbf{r}=0)$$

$$\langle (\log K_{ave}(\vartheta) - \langle \log K_{ave}(\vartheta)\rangle)^2\rangle = \alpha\, C_{\log k}(\mathbf{r}=0)$$

The normalized variance correction factor α given by

$$\alpha = \frac{1}{|\vartheta|^2}\int_\vartheta d^D\mathbf{r}\, d^D\mathbf{r}' \frac{C_{\log k}(\mathbf{r}-\mathbf{r}')}{C_{\log k}(\mathbf{r}=0)},$$

depends only on the geometrical form of the covariance function and on the averaging volume ϑ size λ. It can be observed that it shares the same form than the scale-dependant variance (11) derived before. It can be noticed that using directly LLM formula for estimating K_{eff} for large size λ using these parameters, Eq. (1) under its second form is recovered as terms involving α terms cancel. This highlights some internal consistency of this estimator.

In practice, once the potential is solved, the evaluation of $K_{diss}(\vartheta)$ and $K_{ave}(\vartheta)$ is straightforward and of negligible extra computational cost. For a given size λ, one obtains a set of $(\frac{L}{\lambda})^D$, $D = 2, 3$ values of $K_{diss}(\vartheta)$ and $K_{ave}(\vartheta)$ that can be studied using statistical tools. This will be the main topic of next sections.

6. Numerical methodology

6.1. Generation of media samples

We first compare the formulations over random lognormal media samples with low and high variance, and then, over binary media samples that have a high contrast of characteristic conductivities. We employed a fast Fourier transform (FFT) moving average (FFT-MA) method (Le Ravalec et al., 2000) to generate these samples. Lognormal hydraulic conductivity fields with unitary geometric mean K_g were generated. Gaussian covariance, with an integral scale $I = 16\Delta$ defined as the practical range of the covariance function ($I = \sqrt{3}I_c$), was used to spatially correlate the samples. Fig. 3 (left) shows, as an example, a realization of a lognormal medium obtained with this procedure. All media samples generated have 1024×1024 cells, with a linear size of 1024Δ. In order to reduce the numerical truncation error when computing the potential field, a refining stage of degree 4 was performed (Romeu and Noetinger, 1995; Liu and Wang, 2013), resulting in a grid of 4096×4096 computational cells of linear size $\Delta/4$.

Binary random media is generated as follows: We start by generating a lognormal one with an arbitrary geometric mean K_g and variance $\sigma^2_{\log k}$. Then, this lognormal distribution is binarized using a threshold value k_t, assigning each cell a characteristic k^+ (high conductivity) or k^- (low conductivity) value (with $k^+/k^- = 10^4$). The value of k_t controls the relative population p of high conductivity cells. Three values of p were studied, one at the 2D percolation threshold $p_c = 0.5$, one smaller ($p = 0.4$) and one greater ($p = 0.6$) than p_c. At p_c, 50% of the realizations percolate. We used CONNECT3D software (Pardo-Igúzquiza and Dowd, 2003) to explicitely verify the percolation condition.

The spatial correlation function of the resulting binary medium remains gaussian. In turn, the integral scale of the binary medium is determined by the integral scale of the original lognormal medium, but also by p. To be able to use the former as an input parameter, we've performed an iterative search for each of the values of p studied. Fig. 3 (right) shows, as an example, a realization of such a binary medium.

For each set of parameters, we generated 50 samples in order to obtain an acceptable statistical sampling at largest scale L.

6.2. Potential field calculation

For the K_{ave} and K_{diss} formulations, it is only required to solve the potential in Ω once, and then post-processing of the obtained field is performed to obtain K_{eff} at any scale λ. For the K_{perm} formulation, the potential must be solved independently for all the sub-domains ϑ under study.

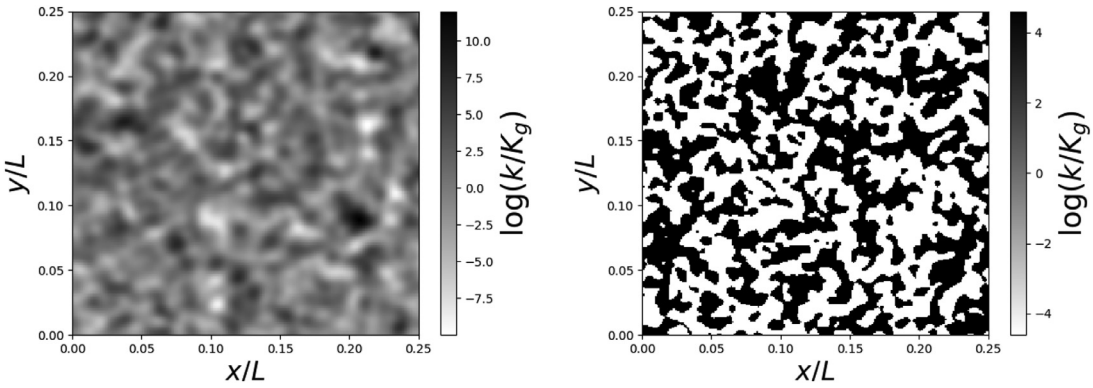

Fig. 3. Maps of $\log(k)$. (left) Lognormal medium obtained from FFTMA. Input data: $\sigma^2_{\log k} = 7$, $I = 16\Delta$. (right) Binary medium. Input data: $p = 0.5$, $k^+/K_g = 100$, $k^-/K_g = 0.01$.

To obtain the potential field we used MODFLOW-2005[1] software (Harbaugh, 2005) with the corresponding boundary conditions. This solver uses the finite difference method with a classical $2D + 1$ point stencil. Particularly, the *Block-Centered Flow package (BCF6)* was used, and the linear equation system was solved with the *Preconditioned Conjugate-Gradient package (PCG)*.

6.3. Implementation of the permeameter scheme

We used classical permeameter boundary conditions in the computation of the potential fields. In MODFLOW, these boundary conditions are applied assigning constant potentials (Dirichlet type) to two opposite cell layers, each of them representing a domain face. A unitary potential difference (ΔP) between them is set. All other faces are constrained by no-flow boundary conditions (Neumann type) applied to ghost cell layers outside the domain. These boundary conditions are applied at $\partial\vartheta$ to compute K_{perm} defined as

$$K_{perm} = \frac{Q}{\lambda\,\Delta P}, \tag{17}$$

The integral of the flow, Q, is calculated at the inlet or the outlet face of the block ϑ with permeameter boundary conditions. For each medium, K_{perm} was computed for the whole set of subscales $\lambda = 2^n$, with integer n between 1 and 10, resulting in $(\frac{L}{\lambda})^2 = 2^{2(10-n)}$ values at each subscale. The same procedure was followed for the other two estimators.

6.4. Implementation of the dissipation scheme

Based on the resulting potential field computed using MODFLOW with permeameter boundary conditions (Sections 6.2 and 6.3) on domain Ω, and the theoretical development presented in Section 5.1, the dissipation-based block estimator computation is as follows. As the finite difference scheme adopted in MODFLOW is cell centered, after solving the potential field in Ω, both the hydraulic conductivity $k_{i,j}$ and potential $P_{i,j}$ at each cell center are known. Notations are referred to cell (i, j) of ϑ, where $(i-1, j)$, $(i+1, j)$, $(i, j-1)$ and $(i, j+1)$ are the left, right, top and bottom neighbouring cells respectively. Using an electrical analogy, the local cell dissipation can be computed as

$$\begin{aligned}\epsilon_{i,j} &= \int_{\vartheta_{i,j}} d^2\mathbf{r}\, k_{i,j}\,(\nabla p)^2 \\ &= 2k_{i,j}\Big[(P_{i+\frac{1}{2},j} - P_{i,j})^2 + (P_{i-\frac{1}{2},j} - P_{i,j})^2 \\ &\quad + (P_{i,j+\frac{1}{2}} - P_{i,j})^2 + (P_{i,j-\frac{1}{2}} - P_{i,j})^2\Big]\end{aligned} \tag{18}$$

The factor $2k_{i,j}$ corresponds to the conductivity of the half bond between the center and any face of $\vartheta_{i,j}$. The potential subscript with minus or plus halves refer to cell face potentials computed invoking the equality of flux at both sides of the face. For example the potential on the left face of cell (i, j) is given by:

$$P_{i-\frac{1}{2},j} = \frac{\left(k_{i,j}P_{i,j} + k_{i-1,j}P_{i-1,j}\right)}{\left(k_{i,j} + k_{i-1,j}\right)}.$$

The other cell face potentials are defined analogously. Using equivalent equations to eliminate face potentials in Eq. (18), we get:

$$\begin{aligned}\epsilon_{i,j} = \frac{1}{2k_{i,j}}\Bigg[&\left(T_{i+\frac{1}{2},j}\,(P_{i+1,j} - P_{i,j})\right)^2 + \left(T_{i-\frac{1}{2},j}\,(P_{i-1,j} - P_{i,j})\right)^2 \\ &+ \left(T_{i,j+\frac{1}{2}}\,(P_{i,j+1} - P_{i,j})\right)^2 + \left(T_{i,j-\frac{1}{2}}\,(P_{i,j-1} - P_{i,j})\right)^2\Bigg].\end{aligned}$$

The coefficients $T_{\cdot,\cdot}$ are the usual intercell harmonic averages given by $T_{i+\frac{1}{2},j} = \frac{2k_{i+1,j}\,k_{i,j}}{k_{i+1,j}+k_{i,j}}$ and $T_{i,j+\frac{1}{2}} = \frac{2k_{i,j+1}\,k_{i,j}}{k_{i,j+1}+k_{i,j}}$.

Ohm's law for dissipation can be recognized through the squares of the fluxes flowing through the faces. The cell face potentials are also used to compute the cell potential gradient as

$$\nabla P^T_{i,j} = \left[\frac{P_{i+\frac{1}{2},j} - P_{i-\frac{1}{2},j}}{\Delta}, \frac{P_{i,j+\frac{1}{2}} - P_{i,j-\frac{1}{2}}}{\Delta}\right].$$

Thus, the averaged potential gradient of the block is

$$\overline{\nabla P} = \frac{\sum_{i,j}\nabla P_{i,j}}{n_i n_j},$$

with n_i, n_j the number of cells in each direction inside the block. In every case, the sum runs over all the fine grid-blocks included in ϑ. Finally, the block dissipation-based estimator of Eq. (15) for block ϑ is computed as

$$K_{diss}(\vartheta) = \frac{\sum_{i,j}\epsilon_{i,j}}{\lambda^2\overline{\nabla P}^2}. \tag{19}$$

Fig. 4 presents the resulting dissipation maps for lognormal and binary media samples. A strong localization (channeling) effect may be noticed close to percolation threshold for the binary case.

6.5. Implementation of the block average conductivity scheme

Based on the computation of the potential field in Ω, the second K_{eff} estimator can be defined in ϑ as:

$$K_{ave} = \frac{\overline{Q}_x}{\lambda\overline{\nabla P}_x}. \tag{20}$$

This expression is based on a large-scale Darcy equation where $\overline{Q}$ is the flow rate and $\overline{\nabla P}$ the potential gradient, both averaged over the domain ϑ of size λ. With the proper boundary conditions it is possible to recover the full hydraulic conductivity tensor (Bauer et al., 2008). In this study, we only considered the direction of the imposed potential difference ΔP.

[1] https://water.usgs.gov/ogw/modflow/mf2005.html

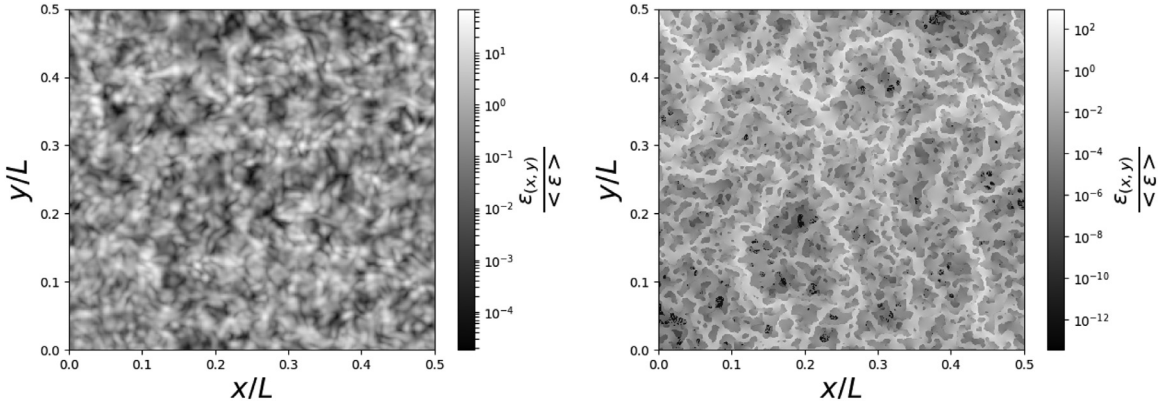

Fig. 4. Local dissipation (ϵ) maps: (left) lognormal medium with $\sigma^2_{\log k} = 7$ and (right) binary medium with $p = 0.5$.

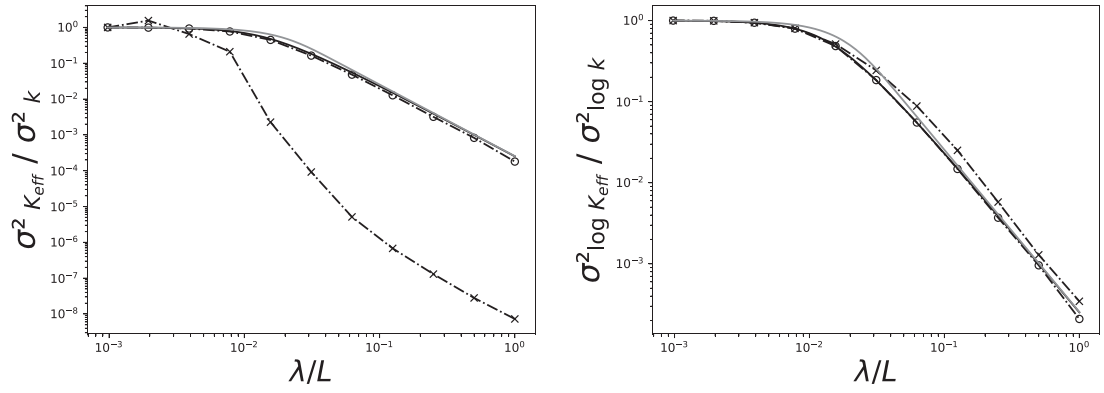

Fig. 5. Analytical and numerical results for Gaussian covariance media. (Left) $\sigma^2_{K_{eff}}$ compared against Eqs. (13) and (14). (Right) $\sigma^2_{\log K_{eff}}$ compared against Eqs. (13) and (14) using the mean-field approximation. (-.-) Numerical; (—) Analytical; (—) Simplified analytical. Input variance: (∘) $\sigma^2_{\log k} = 0.1$, (x) $\sigma^2_{\log k} = 7$.

Table 1
Simulation parameter names, definitions and values.

Definition	Symbol	Values	
		Lognormal	Binary
Size of the full domain	L	1024Δ	
Covariance function	$C(\mathbf{r})$	Gaussian	
Integral scale	I	16Δ	8Δ
Fine grid geometric mean K_g $[m/day]$	K_g	1	
Fine grid variance of $\log(K)$	$C_{\log k}(r=0) = \sigma^2_{\log k}$	0.1; 7	
Characteristic conductivity $[m/day]$	k^+; k^-		100; 0.01
Proportion of cells with k^+	p		0.4; 0.5; 0.6

7. Results

We begin this section by comparing, as a form of validation, the outcomes of the analytical developments of Section 4, for lognormal media, with the corresponding numerical results using the well-known K_{perm} estimator. Then, for both type of media, we study the scale-dependence of the pdf of the three proposed estimators, to later focus on the first two gaussian moments i.e. mean and variance. For this latter case, a comparison with the mean-field analytical variance of K_{eff}, Eq. (13), is performed. The common parameters and values used in the simulations are presented in Table 1.

7.1. Comparison of the different analytical expressions for $C_{K_{eff}}(\lambda)$ with numerical results

Fig. 5 shows the variance of K_{eff} given by Eqs. (13) and (14), and their equivalent expressions within the mean-field approximation, compared with the K_{perm} estimator, as a function of the coarsening scale λ, that varies between fine grid scale Δ and L. A low ($\sigma^2_{\log k} = 0.1$) and a high ($\sigma^2_{\log k} = 7$) fine grid variance are used as extreme cases.

The analytical results are in good agreement with the numerical simulations for $\sigma^2_{\log k} = 0.1$ when using the expressions based on the conductivity variance $\sigma^2_{K_{eff}}$ (Eqs. (13) and (14)). The difference increases for the case of $\sigma^2_{\log k} = 7$, specially for scales equal or greater than the integral scale, defined as the practical range of the covariance function. The estimation of the variance of the logarithm, $\sigma^2_{\log K_{eff}}$ (Appendix C.1) provides a better agreement with the numerical results even for $\sigma^2_{\log k} = 7$. In this case, the analytical equations correctly capture the tendency as the scale increases, with small discrepancy from the numerical results beyond the integral scale. In both cases, the simplified formulas (Eq. (14)) coincide to a large extent with the complete ones except at the scales close to the integral scale, where a small difference appears. In view of these

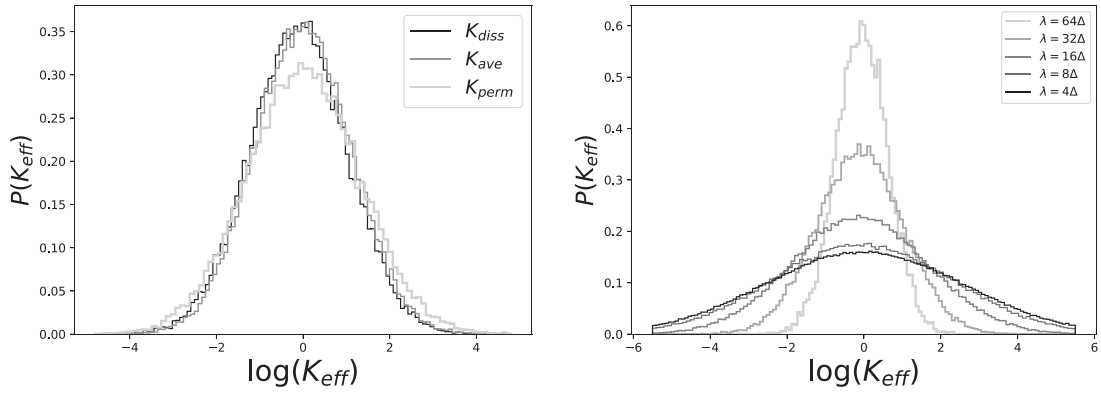

Fig. 6. Pdf's of $\log(K_{eff})$. Input data: $\sigma^2_{\log k} = 7$, I=16Δ. (Left) For the three estimators at $\lambda = 32\Delta$. (Right) Pdf of K_{diss} for $\lambda = 4$, 8, 16, 32 and 64Δ.

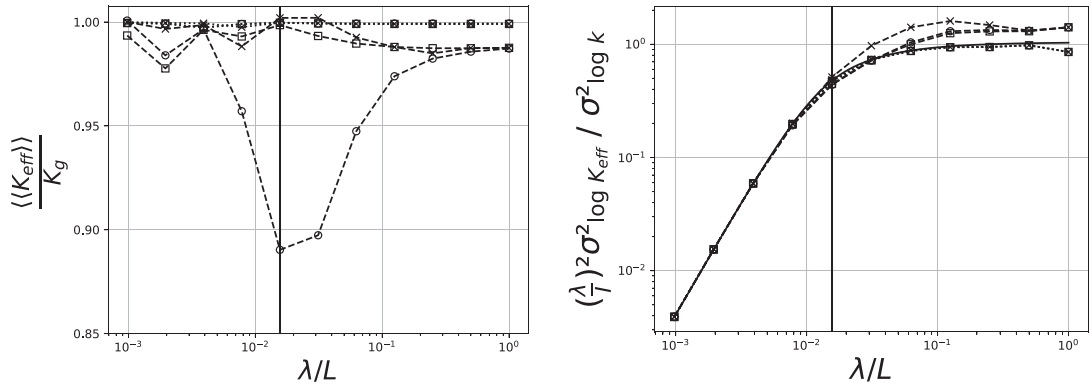

Fig. 7. K_{eff} as a function of λ, for the three estimators,for lognormal media: (left) geometric mean and (right) rescaled variance $\frac{\lambda^2}{I^2}C_{\log K_{eff}}$. Input variance: (....) $\sigma^2_{\log k} = 0.1$, (–) $\sigma^2_{\log k} = 7$. Upscaling method: (x) K_{perm}, (∘) K_{diss}, (□) K_{ave}. The vertical line indicates the integral scale. (—) Analytical variance Eq. (13) using the mean-field approximation.

observations, comparison against analytical results in the next sections will be only carried out with respect to Eq. (13) using the mean-field approximation.

7.2. Lognormal media

7.2.1. Probability density function of the different estimators

Pdf's of K_{diss}, K_{ave} and K_{perm} are plotted in Fig. 6 (left) for $\sigma^2_{\log k} = 7$. Although K_{diss} and K_{ave} present a sharper pdf, they are rather similar. The dependence of the pdf of K_{diss} with the coarsening scale λ is shown in Fig. 6 (right). It can be observed that the pdf remain Gaussian at all scales. As a Gaussian pdf is fully described by its mean and variance, in the following subsection, we focus our attention on these two moments.

7.2.2. Scale dependence of the mean and variance of K_{eff}

Fig. 7 compares the values of the geometric mean of K_{eff}, indicated by $\langle\langle \dots \rangle\rangle$ (left), and the variance $\sigma^2_{\log K_{eff}}$ scaled by $(\frac{\lambda}{I})^2$ (see Appendix C) (right) for the three estimators. As λ tends to Δ, $\langle\langle K_{eff}\rangle\rangle$ approaches to the fine scale mean K_g for both variances. For $\sigma^2_{\log k} = 0.1$, the three formulations yield very similar results, while for $\sigma^2_{\log k} = 7$ some discrepancies are observed. Moreover, for λ close to I, a depart from the theoretical value (of upto 12%) is observed for K_{diss}. We recall that, as developed in Section 5.1.1, if $\vartheta = \Omega$, the potential gradients transverse to the mean flow vanish, due to the boundary conditions applied at that scale in all cases, but, if $\vartheta < \Omega$, these gradients may exist and be non negligible. Also, they are stronger as the heterogeneity increases, explaining the slump in K_{diss} for λ close to I.

The variances of K_{eff} were evaluated analytically using the mean-field approximation of Eq. (13). In Fig. 7 (right), the variances of the three estimators show an excellent agreement with the analytical results for $\sigma^2_{\log k} = 0.1$, while, for $\sigma^2_{\log k} = 7$, a slight difference for $\lambda > I$ is observed for the three estimators, probably due to discretization effects (Romeu and Noetinger, 1995).

7.3. Binary media

7.3.1. Probability density functions of the K_{eff} estimators

In binary media, the lower limiting case is when the upscaling scale λ tends to the fine grid scale Δ, with only two possible conductivity values: k^+ with probability p, and k^- with probability $(1-p)$. Consequently, the pdf of the effective conductivity tends to a two-peaked distribution with relative heights given by p and $(1-p)$, and its mean is similar to that of the original medium at the fine grid scale. On the other hand, the upper limit correspond to the upscaling scale reaching the domain scale L. In this case, the pdf of the effective conductivity looks more like a unimodal distribution with its mean approaching k^+ when $p > p_c$, and k^- when $p < p_c$. At intermediate scales, a transition between both extreme behaviors occurs. Pdf's of K_{diss}, K_{ave} and K_{perm} are plotted in Fig. 8 in order to compare them with the expected behavior. Three situations, with p smaller, close to and greater than $p_c = 0.5$ (for which percolation transition occurs), are shown in this figure.

In the left column of the figure, the three methods are compared for $\lambda = 32\Delta$. At this intermediate scale different behaviors are observed depending on the method. The pdf's of the three estimators considered here exhibit some differences: the K_{perm} estimator presents more peaked

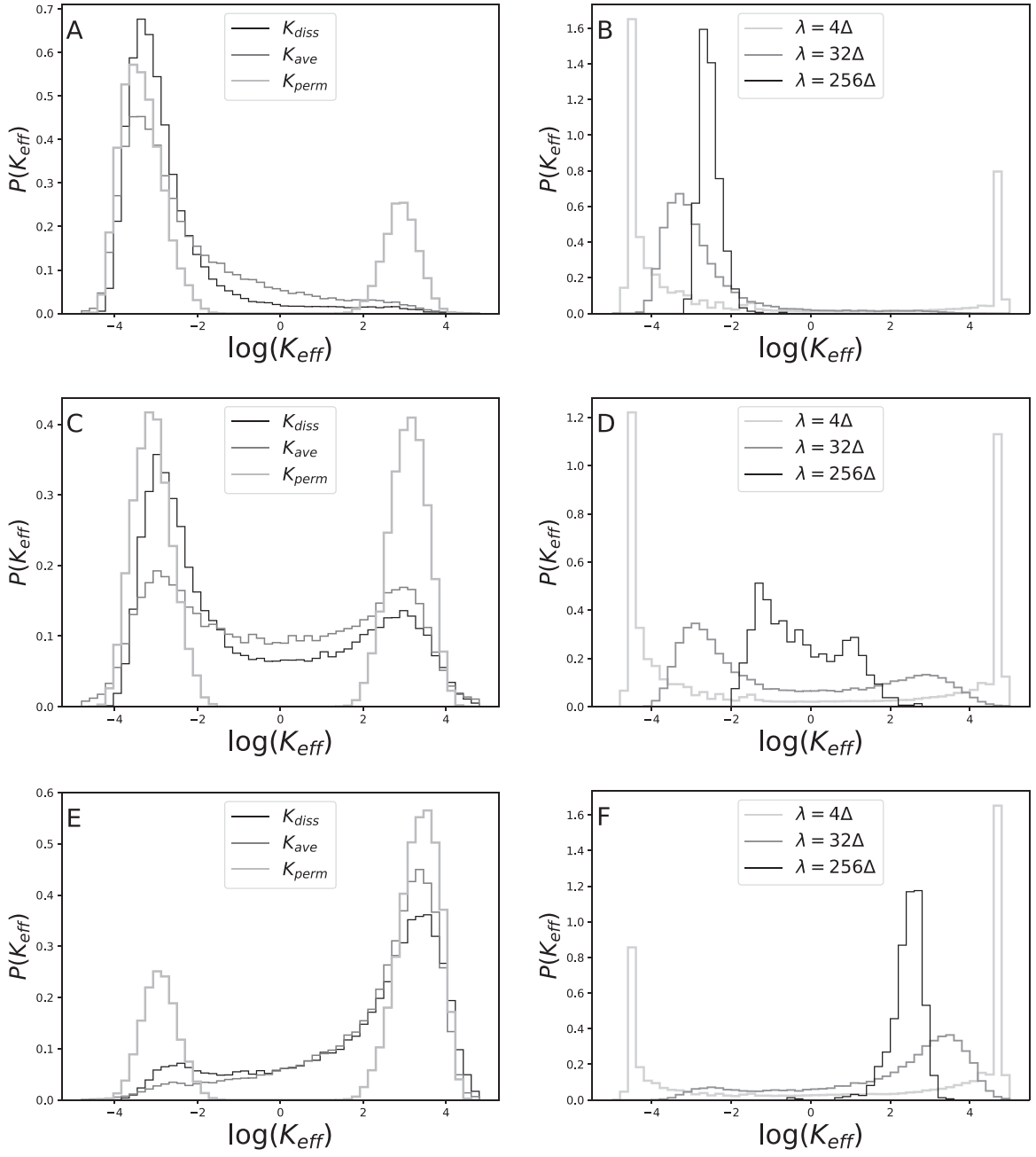

Fig. 8. Pdf's of the effective conductivity $\log(K_{eff})$ resulting from the three studied estimators. Input data: relative population $p = 0.4$, $p = 0.5$ and $p = 0.6$ (top to bottom). (Left) Results obtained with the three methods for $\lambda = 32\Delta$. (Right) K_{diss} results for three block sizes $\lambda = 4$, 32, and 256 Δ.

distributions with two clearly separated modes while those of global methods, K_{diss} and K_{ave}, are relatively more homogeneous, with a continuous variation between the peaks. Also, the values of conductivity corresponding to the facies that does not percolate are only retained in the case of K_{perm}, while K_{diss} and K_{ave} smooth them out. This is a direct effect of the permeameter boundary conditions that are imposed for each sub domain ϑ when computing K_{perm}. This renders percolation in ϑ much more critical for K_{eff}. On the other hand, analyzing the behavior when small, middle and large scales are adopted for λ, the expected behavior is recovered. K_{diss} converges to an unimodal distribution as λ increases, faster as p departs from p_c, as it was observed in a previous study for K_{perm} (Boschan and Noetinger, 2012). In addition, as p departs from p_c, for a given λ, the distributions become narrower. This implies that the convergence to a representative mean is slower near percolation.

7.3.2. Scale dependence of the mean and variance of K_{eff}

In the binary case, as it is clearly seen in Fig. 8, the pdf's of K_{eff} are far from being unimodal, and then, the mean and variance become less representative of the pdf, compared with the lognormal case (cf. Section 7.2.1). For example, one may note that, in panel C of Fig. 8, the mean would not be particularly representative. However, previous studies analyzed the mean and variance much more frequently than the complete pdf, so we consider interesting to present them for comparison.

Fig. 9 shows the variation of geometric mean of K_{eff} (left), and of the variance $\sigma^2_{\log K_{eff}}$ (right), for the three estimators, as a function of λ for $p = 0.4$, $p = 0.5$ and $p = 0.6$. The values of $\langle\langle K_{eff}\rangle\rangle$ coincide as λ tends to the limiting Δ or L, for all the values of p. The behavior at both limits of the range corresponds to which is expected for a representative effective conductivity. Furthermore, the behavior far from those extreme values

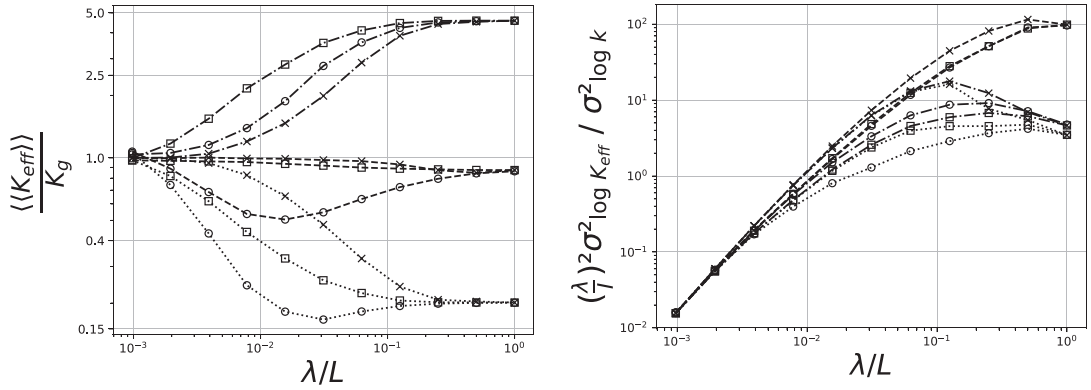

Fig. 9. Dependence of the three estimators of K_{eff} with the scale in binary media: (left) geometric mean and (right) rescaled variance $\frac{\lambda^2}{I^2}C_{\log K_{eff}}$. Input data: (....) $p = 0.4$, (–) $p = 0.5$, (-.-) $p = 0.6$. Upscaling method: (x) K_{perm}, (∘) K_{diss}, (□) K_{ave}.

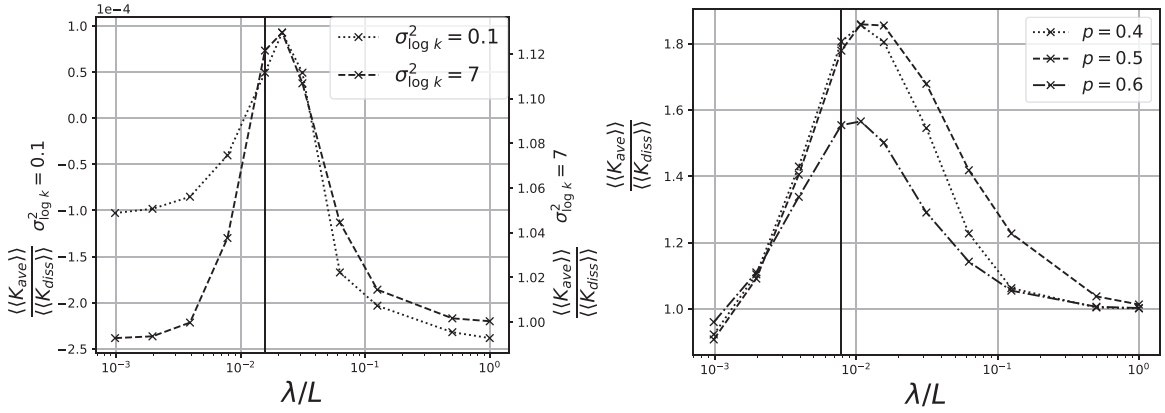

Fig. 10. Discrepancy between the geometric mean of K_{diss} and that of K_{ave}. (Left) Results for lognormal media, Section 7.2.2. (Right) Results for binary media, Section 7.3.2. (|) Integral scale.

is strongly dependent on the particular estimator. As observed in Fig. 8, the two peaks in the K_{perm} histogram remained clearly identifiable at larger λ values, in opposition to what happened in the cases of K_{diss} or K_{ave}. The outcome is that if p is far from p_c, K_{perm} converges more slowly than K_{diss} or K_{ave} to the asymptotic value of $\lambda = L$. This is consistent with the faster homogenization shown by the global estimators in the pdf's of section 7.3.1. Comparing K_{diss} and K_{ave}, the former shows a slight bias to lower $\langle\langle K_{eff}\rangle\rangle$ values.

The variance $\sigma^2_{\log K_{eff}}$ computed using the three formulations also coincides as λ tends to Δ or L. At intermediate scales, K_{perm} always yields the highest $\sigma^2_{\log K_{eff}}$, in agreement with the findings shown in Section 7.3.1, where it was shown that the pdf remained bimodal for a greater λ than for the other two methods. Note that, in the non percolating case ($p = 0.4$), K_{diss} produces lower variances than K_{ave}, while the opposite happens for the percolating case ($p = 0.6$), and, at $p_c = 0.5$, both estimators yield similar values of $\sigma^2_{\log K_{eff}}$.

8. Summary, discussion and perspectives

After introducing an efficient K_{eff} estimator based on energy dissipation, we revisited numerically and analytically three of the most important upscaling formulations, analyzing the scale dependence of the resulting K_{eff} distributions.

For 2D lognormal media, K_{eff} distributions remain lognormal at intermediate coarsening scales for all the formulations, a result that could be theoretically related to the LLM formula (Landau and Lifshitz, 1960; Matheron, 1967). The numerical results for $\langle\langle K_{eff}\rangle\rangle$ and $\sigma^2_{\log K_{eff}}$ are in agreement with the analytical ones. This is notable for intermediate coarsening scales, having in mind that these last results are not exact. In particular, the asymptotic behavior of $\sigma^2_{\log K_{eff}}$ for $\lambda > I$, varying as $(1/\lambda)^2$, is reminiscent to a central limit theorem.

In the binary case, for p far from p_c, the pdf of K_{eff} evolves from a bimodal to a unimodal distribution, with representative mean and variance. The mean and variance of the three estimators converge to the same asymptotic K_{eff} values for $p = 0.4$ or 0.6. It can be observed that the latter obeys the scaling law with $1/\lambda^2$ in that case. Close to percolation threshold p_c, the intermediate-scale K_{eff} distributions do not exhibit convergence to an asymptotic stable distribution. The $\langle\langle K_{eff}\rangle\rangle$ remains close to the fine grid geometric mean K_g. This may be explained by the fact that in 2D, at $0.5 = p_c$, the analytical result of Matheron (1967) can be applied, yielding the geometric average in that very specific case. Looking more carefully to Fig. 9, for $p = p_c$, $\sigma^2_{\log K_{eff}}$ does not follow the scaling law in $1/\lambda^2$. This should be related to the absence of a representative elementary volume (Berkowitz and Balberg, 1993; Hunt et al., 2014; Stauffer and Aharony, 2014). Quantification of such effects remains to be studied, and K_{eff} estimators that comply to finite size scaling arguments might improve the existing description.

The computation of K_{eff} through K_{ave} and K_{diss} is much more efficient than using K_{perm}, because, in this case, the potential is solved once for Ω, and then by post-treating this solution, K_{eff} can be obtained at all scales if a multiscale description is required, while providing similar results. Using K_{perm} involves solving the potential independently for each scale, due to the strong influence of the boundary conditions imposed at $\partial\vartheta$.

Now comparing K_{ave} and K_{diss}, we illustrate the degree of discrepancy between these two estimators as a function of the coarsening scale, showing in Fig. 10 the ratio between the geometric mean of K_{ave} and that

of K_{diss}. It can be observed that the greater discrepancy occurs, both for lognormal and binary media, for $\lambda \approx I$, where I is the practical range of the covariance function as measured in both types of media samples, giving a characteristic lengthscale for heterogeneity. Note that K_{diss} (see Section 5.1) is sensible to transverse potential gradients, while K_{ave} isn't, because it assumes a colinearity between potential gradient and flow. These transverse potential gradients vanish at $\lambda = \Delta$ and at $\lambda = L$, while they have a maximum in-between, at a critical lengthscale, despite that media samples are statistically isotropic. The degree of discrepancy is then probably driven by the scale dependence of these transverse potential gradients.

Except for the lognormal case of $\sigma^2_{\log k} = 0.1$, K_{diss} is smaller than K_{ave} up to 12% in the lognormal case of $\sigma^2_{\log k} = 7$, and up to 80% in the binary case. The bias of K_{diss} towards lower values was also observed in the pdf's shown in the Sections 7.2.1 and 7.3.1.

The 3D generalization of this work is currently under development. In particular, the appearance of an attractive conductivity distribution for the different formulations, playing in 3D an analogous role to the lognormal distribution in 2D, is of central interest. Moreover, for binary media, it is highly interesting to assess the slower convergence to an homogeneous K_{eff} distribution close to the percolation transition in 3D media in the context of the different formulations. More realistic or complex distributions such as non Gaussian or power-law (Panzeri et al., 2016; Riva et al., 2017; Guadagnini et al., 2018) will be addressed in future work. A major practical issue regarding non-homogeneous materials is to find some self-contained estimation of the REV size allowing to determine, for a given case, if the REV size is reached. That will help to find the optimal meshing size, and to quantify uncertainty propagation.

Declaration of Competing Interest

The authors declare that they have no known competing financial interests or personal relationships that could have appeared to influence the work reported in this paper.

CRediT authorship contribution statement

Iván Colecchio: Conceptualization, Data curation, Formal analysis, Writing - original draft. **Alejandro Boschan:** Conceptualization, Data curation, Formal analysis, Writing - original draft. **Alejandro D. Otero:** Conceptualization, Data curation, Formal analysis, Writing - original draft. **Benoît Noetinger:** Conceptualization, Data curation, Formal analysis, Writing - original draft.

Acknowledgments

The authors would like to acknowledge the computational time from the TUPAC cluster made available by the *CSC-CONICET* for conducting this research.

Appendix A. Functional differentiation

Functional differentiation is a generalization of calculus to functionals, i.e., functions having a function as argument. Our presentation is intuitive. Let $F(\{k\})$ be a functional that depends on the whole set of values of k which is an arbitrary function of position $\mathbf{r} \in \mathbf{\Omega}$. The notation $\{\ldots\}$ recalls that F is a functional. Examples of functional can be the value of field k at a given location $\mathbf{r}_0$: $F_0(\{k\}) = k(\mathbf{r}_0)$, the weighted average $F_{<\ldots>_f}(\{k\}) = \frac{1}{|V|}\int_V d^D\mathbf{r}\ f(\mathbf{r})\ k(\mathbf{r})$ in which $f(\mathbf{r})$ is a fixed function that does not depend on k. The functional derivative of a functional $F(\{k\})$ is defined by the following equation:

$$Lim_{\epsilon\to 0}\frac{F(\{k+\epsilon\delta k\}) - F(\{k\})}{\epsilon} = \int_V d^D\mathbf{r}\,\frac{\delta F}{\delta k(\mathbf{r})}\delta k(\mathbf{r})$$

Here, δk is an arbitrary perturbation. The functional derivative has a supplementary spatial argument (that corresponds in the case of partial derivatives to the choice of the variable with respect to which the derivative is performed). In the examples of $F_0(\{k\})$ and $F_{<\ldots>_f}(\{k\})$, one has

$$\frac{\delta F_0}{\delta k(\mathbf{r})} = \delta((\mathbf{r} - \mathbf{r}_0)$$

$$\frac{\delta F_{<\ldots>_f}}{\delta k(\mathbf{r})} = \frac{f(\mathbf{r})}{|V|}$$

It gives the sensibility of the variation of F with respect to a local variation of its argument k at position $\mathbf{r}$. Nth order functional derivatives can be defined, as well as a Taylor formula, replacing summations by integrations.

If $f(x)$ is a standard differentiable real function, one has the chain derivative formula:

$$\frac{\delta f(F)}{\delta k(\mathbf{r})} = \frac{df}{dx}(F)\ \frac{\delta F}{\delta k(\mathbf{r})}$$

If $p(\mathbf{r})$ obeys a Laplace equation such as

$$\nabla\cdot(k(\mathbf{r})\ \nabla p(\mathbf{r})) = 0,$$

Putting $k(\mathbf{r}) = k + \delta k(\mathbf{r})$, one obtains:

$$\nabla\cdot[(k+\delta k(\mathbf{r}))\ (\nabla p(\mathbf{r}) + \nabla\delta p(\mathbf{r}))] = 0,$$

Denoting by $\delta p(\mathbf{r})$ the first order variation of potential $p(\mathbf{r})$ with respect to $k(\mathbf{r})$, one obtains that $\delta p(\mathbf{r})$ obeys the following equation, valid at first order:

$$\nabla\cdot(k\ \nabla\delta p(\mathbf{r})) = -\nabla\cdot[\delta k(\mathbf{r})\ \nabla p(\mathbf{r})] \tag{A.1}$$

As the unperturbed potential $p(\mathbf{r})$ fulfills the boundary conditions at the domain boundary, $\delta p(\mathbf{r}) = 0$ on Dirichlet boundaries, and same conditions for the normal flux at the Neumann boundaries. This equation has the formal solution:

$$\delta p(\mathbf{r}) = -\int_V d^D\mathbf{r}'\ G_k(\mathbf{r},\mathbf{r}')\ \nabla\cdot\left[\delta k(\mathbf{r}')\ \nabla p_0(\mathbf{r}')\right]. \tag{A.2}$$

Here, $G_k(\mathbf{r}, \mathbf{r}')$ is the Green's function of the Laplace operator that obeys the following equations, to be supplemented by consistent boundary conditions:

$$\nabla\cdot\left(k\ \nabla G_k(\mathbf{r},\mathbf{r}')\right) = \delta(\mathbf{r}-\mathbf{r}')$$

$$G_k(\mathbf{r}_\mathbf{x} = 0,1,\mathbf{r}') = 0, \qquad \partial_y G_k(\mathbf{r}_\mathbf{y} = 0,1,\mathbf{r}') = 0$$

So one gets finally after one integration by parts:

$$\frac{\delta p(\mathbf{r})}{\delta k(\mathbf{r}')} = \nabla_{\mathbf{r}'}G_k(\mathbf{r},\mathbf{r}')\cdot\nabla p_0(\mathbf{r}') \tag{A.3}$$

This result may recovered directly, applying the operator $\frac{\delta\cdot}{\delta k(\mathbf{r}')}$ at both sides of Eq. (3), providing:

$$\nabla\cdot\left(k\ \nabla\frac{\delta p(\mathbf{r})}{\delta k(\mathbf{r}')}\right) = -\nabla\cdot[\delta((\mathbf{r}'-\mathbf{r})\ \nabla p(\mathbf{r})],$$

which is equivalent to Eq. (A.3). Note that the base conductivity field k may also depend on position, or be equal to $\langle k\rangle$, the choice depends on the application at hand.

Appendix B. Second order estimation of the average effective conductivity

In order to illustrate the functional formalism, we carry out with this tool the classical second order expansion of the effective conductivity (Dagan, 1989). The Taylor expansion Eq. (10), gives directly a second order series expansion that will provide the desired expansion after averaging:

$$\langle K_{eff}\rangle = \langle k\rangle + \frac{1}{2}\int_\Omega d^D\mathbf{r}\ d^D\mathbf{r}'\ \frac{\delta^2 K_{eff}}{\delta k(\mathbf{r})\delta k(\mathbf{r}')}\ C_k(\mathbf{r}'-\mathbf{r}). \tag{B.1}$$

The main task is to evaluate explicitly the second order functional derivative that may be simplified in the following form, using Eq. (C.1) differentiated once more time:

$$\frac{\delta^2 K_{eff}}{\delta k(\mathbf{r})\,\delta k(\mathbf{r}')} = \frac{1}{|\Omega|} 2\nabla p_0(\mathbf{r}).\nabla \frac{\delta p(\mathbf{r})}{\delta k(\mathbf{r}')}$$

In that equation, $p_0(\mathbf{r})$ is the non-perturbed potential. The derivative $\frac{\delta p(\mathbf{r})}{\delta k(\mathbf{r}')}$ is given by Eq. (A.2). So, we get after substitution:

$$\frac{\delta p(\mathbf{r})}{\delta k(\mathbf{r}')} = \frac{1}{\langle k\rangle}\nabla G(\mathbf{r},\mathbf{r}')\cdot\nabla p_0(\mathbf{r}'). \tag{B.2}$$

In that expression, $G(\mathbf{r}, \mathbf{r}')$ is the Green's function of Laplace operator ∇^2, this explains the factor $\frac{1}{\langle k\rangle}$. Note that due to the boundary conditions that break full translational invariance of the system, this Green's function does not depend only on the argument $(\mathbf{r}-\mathbf{r}')$. Gathering these results in Eq. (B.1), and using the fact that $\nabla p_0(\mathbf{r}) = e_x$, one obtains:

$$\begin{aligned}\langle K_{eff}\rangle &= \langle k\rangle - \frac{1}{\langle k\rangle|\Omega|}\int_\Omega d^D\mathbf{r}\, d^D\mathbf{r}'\, \nabla p_0(\mathbf{r}).\nabla\frac{\delta p(\mathbf{r})}{\delta k(\mathbf{r}')}\, C_k(\mathbf{r}'-\mathbf{r})\\ &= \langle k\rangle - \frac{1}{\langle k\rangle|\Omega|}\int_\Omega d^D\mathbf{r}\, d^D\mathbf{r}'\, \partial_{r_x}\partial_{r'_x} G(\mathbf{r},\mathbf{r}')C_k(\mathbf{r}'-\mathbf{r})\end{aligned} \tag{B.3}$$

Assuming that $|\Omega|^{1/D}$ is large compared with the integral scale I, one can replace $G(\mathbf{r}, \mathbf{r}')$ by the free space Green's function $G(\mathbf{r}-\mathbf{r}')$. This is equivalent to estimate the Green's function assuming that the boundary conditions are rejected at infinity.

Using the correlation function isotropy, the integral can be simplified using a classical trace argument, yielding:

$$\langle K_{eff}\rangle = \langle k\rangle - \frac{1}{\langle k\rangle}\frac{1}{D}C_k(\mathbf{r}=0).$$

Up to the same order of approximation, this formula can be rewritten on a more usual form as:

$$\langle K_{eff}\rangle = \exp\langle\log(k)\rangle e^{(\frac{1}{2}-\frac{1}{D})C_{\log k}(\mathbf{r}=0)}.$$

For log normal media, this formula is equivalent to the LLM conjecture, Eq. (1). The second order expansion is thus recovered for large averaging volumes, with a quite concise calculation.

Appendix C. Second order estimation of the variance of the effective conductivity

The variance of the effective conductivity is given by

$$C_{K_{eff}}(L) = \langle K_{eff}^2\rangle - \langle K_{eff}\rangle^2 = \langle(K_{eff} - \langle K_{eff}\rangle)^2\rangle.$$

Using the Taylor expansion Eq. (10), and keeping only second order terms, one gets dropping the averaging symbol $\langle\cdots\rangle$ under the integral sign, a procedure that is straightforward within the stochastic context (Dagan, 1989; Gelhar, 1993; Hristopulos, 2020). The procedure would be different using a volume averaging technique involving boundary of averaging-volume corrections, Hassanizadeh and Gray (1979), Whitaker (2013):

$$C_{K_{eff}}(L) = \int_\Omega d^D\mathbf{r}\, d^D\mathbf{r}'\left\langle \frac{\delta K_{eff}}{\delta k(\mathbf{r})}\frac{\delta K_{eff}}{\delta k(\mathbf{r}')}\,\delta k(\mathbf{r})\,\delta k(\mathbf{r}')\right\rangle + \ldots$$

The quantity $\frac{\delta K_{eff}}{\delta k(\mathbf{r})}$ can be written under a simple form:

$$\frac{\delta K_{eff}}{\delta k(\mathbf{r})}\,\overline{\nabla p}^2_{\Omega,x}\,|\Omega| = \nabla p(\mathbf{r})^2. \tag{C.1}$$

Derivation of Eq. (C.1) is straightforward using the variational characterization Eq. (9) that can be differentiated directly with respect to $\delta k(\mathbf{r})$ ignoring the implicit dependence of $\nabla p(\mathbf{r})^2$ with $\delta k(\mathbf{r})$ that is known to vanish thanks to the variational characterization. This Eq. (C.1) relates the influence of a local hydraulic conductivity change on K_{eff} to the local potential gradient. This result was already derived using similar methods by Jacquard (1965) and generalized to obtain shape derivatives of effective conductivity with respect to geometrical shape of inclusions by Noetinger (2013). One can remark that in a location where $\nabla p(\mathbf{r}) = 0$, the local conductivity has no influence at all on the large scale conductivity: it is screened by other patterns that imply that there is no flow at this location. This is a rather intuitive result.

Thus using Eq. (C.1), we obtain:

$$C_{K_{eff}}(L) = \frac{1}{|\Omega|^2}\int_\Omega d^D\mathbf{r}\, d^D\mathbf{r}'\left\langle \frac{\nabla p(\mathbf{r})^2}{\overline{\nabla p}^2_{\Omega,x}}\frac{\nabla p(\mathbf{r}')^2}{\overline{\nabla p}^2_{\Omega,x}}\,\delta k(\mathbf{r})\,\delta k(\mathbf{r}')\right\rangle + \ldots \tag{C.2}$$

As we are seeking a second order expansion of the variance of effective conductivity, the local quantity $\frac{\nabla p(\mathbf{r})^2}{\overline{\nabla p}^2_{\Omega,x}}$ (resp. $\frac{\nabla p(\mathbf{r}')^2}{\overline{\nabla p}^2_{\Omega,x}}$) may be replaced by 1, getting:

$$C_{K_{eff}}(L) = \frac{1}{|\Omega|^2}\int_\Omega d^D\mathbf{r}\, d^D\mathbf{r}'\,\langle\delta k(\mathbf{r})\,\delta k(\mathbf{r}')\rangle. \tag{C.3}$$

After averaging, introducing the pair correlation function $C_k(\mathbf{r}-\mathbf{r}') = \langle\delta k(\mathbf{r})\,\delta k(\mathbf{r}')\rangle$ of the hydraulic conductivity fluctuations, we get a formula already obtained by Rubin and Gómez-Hernández (1990), Sánchez-Vila et al. (1995), Wen and Gómez-Hernández (1996):

$$C_{K_{eff}}(L) = \frac{1}{|\Omega|^2}\int_\Omega d^D\mathbf{r}\, d^D\mathbf{r}'\, C_k(\mathbf{r}-\mathbf{r}'). \tag{C.4}$$

Note that for small averaging volume size L compared to the integral scale I, this formula gives by direct inspection $C_{K_{eff}}(L) = C_k(r=0)$. On the other limit, assuming that the unit volume size is very large compared to the underlying integral scale, one gets the asymptotic behavior:

$$C_{K_{eff}}(L) \approx \frac{1}{|\Omega|}\int_\Omega d^D\mathbf{r}\, C_k(\mathbf{r}). \tag{C.5}$$

For large L, one has the scaling :

$$\frac{L^D}{I^D}C_{K_{eff}}(L) \approx \int_\Omega d^D\mathbf{r}\,\frac{C_k(\mathbf{r})}{I^D}. \tag{C.6}$$

The factor L^D/I^D corresponds to the number of independent statistical units that belong to volume Ω. This scaling corresponds thus to a central limit theorem characterizing the emergence of a deterministic large scale effective conductivity. In other words, the system exhibits self averaging properties. Eqs. (C.4) and (C.5) are solved for the particular case of the Gaussian covariance in C.2.

C1. Improved estimation of the variance, mean-field approximation

The preceding development is limited to small variances. In order to find an improved approximation, one can use Eq. (C.2) written on an equivalent form:

$$\begin{aligned}\langle K_{eff}^2\rangle - \langle K_{eff}\rangle^2 = \frac{1}{|\Omega|^2}\int_\Omega d^D\mathbf{r}\, d^D\mathbf{r}'\\ \left\langle \frac{k(\mathbf{r})\nabla p(\mathbf{r})^2}{\overline{\nabla p}^2_{\Omega,x}}\frac{k(\mathbf{r}')\nabla p(\mathbf{r}')^2}{\overline{\nabla p}^2_{\Omega,x}}\frac{\delta k(\mathbf{r})}{k(\mathbf{r})}\frac{\delta k(\mathbf{r}')}{k(\mathbf{r}')}\right\rangle + \ldots\end{aligned}$$

Now, one can replace $k(\mathbf{r})\nabla p(\mathbf{r})^2$ and $k(\mathbf{r}')\nabla p(\mathbf{r}')^2$ by their common average value $\langle K_{eff}\rangle\overline{\nabla p}^2_{\Omega,x}$. So one gets:

$$\frac{\langle K_{eff}^2\rangle - \langle K_{eff}\rangle^2}{\langle K_{eff}\rangle^2} = \frac{1}{|\Omega|^2}\int_\Omega d^D\mathbf{r}\, d^D\mathbf{r}'\langle\frac{\delta k(\mathbf{r})}{k(\mathbf{r})}\frac{\delta k(\mathbf{r}')}{k(\mathbf{r}')}\rangle + \ldots$$

Up to this order of approximation, the result can be identified with the variance of $\log(K_{eff})$ and the equation can be rewritten as:

$$\begin{aligned}C_{\log K_{eff}}(L) &= \langle(\log(K_{eff}))^2 - \langle\log(K_{eff})\rangle^2\rangle\\ &= \frac{1}{|\Omega|^2}\int_\Omega d^D\mathbf{r}\, d^D\mathbf{r}'\langle\delta\log k(\mathbf{r})\,\delta\log k(\mathbf{r}')\rangle + \ldots\end{aligned}$$

This equation, up to this order of approximation, is equivalent to Eq. (C.4), by replacing every occurrence of a conductivity by the corresponding logarithm, so:

$$C_{\log K_{eff}}(L) = \frac{1}{|\Omega|^2}\int_\Omega d^D\mathbf{r}\, d^D\mathbf{r}' C_{\log k}(\mathbf{r}-\mathbf{r}'). \tag{C.7}$$

The resulting formula is similar to Eq. (C.4), replacing the covariance function by the log conductivity covariance function. For the special case of lognormal media, this is a quite natural transformation. The same can be done with the simplified formula (C.5).

C2. Gaussian covariance case

In the isotropic Gaussian case, the covariance function is given by

$$C_k(\mathbf{r}) = C_k(r=0)\, e^{-\frac{r^2}{2I_c^2}}$$

The integral factorizes, and after changing variables $x \to x/I_c$, we obtain:

$$\begin{aligned} C_{K_{eff}(L)} &= C_k(r=0)\left(\frac{I_c}{L}\right)^{2D}\left[\int_{-L/2I_c}^{L/2I_c}\int_{-L/2I_c}^{L/2I_c} dx\, dy\, e^{-\frac{(x-y)^2}{2}}\right]^D \\ &= C_k(r=0)\left(\frac{I_c}{L}\right)^{2D}\left\{\sqrt{\frac{\pi}{2}}\int_{-L/2I_c}^{L/2I_c} dy\left[\mathrm{erf}\left(\frac{L/I_c-2y}{2\sqrt{2}}\right)\right.\right. \\ &\quad \left.\left. + \mathrm{erf}\left(\frac{L/Ic+2y}{2\sqrt{2}}\right)\right]\right\}^D \\ &= C_k(r=0)\left(\frac{I_c}{L}\right)^{2D}\left[\sqrt{2\pi}\frac{L}{I_c}\,\mathrm{erf}\left(\sqrt{2}\frac{L}{I_c}\right) + 2e^{-\frac{L^2}{2I_c^2}} - 2\right]^D \end{aligned} \tag{C.8}$$

Considering small upscaling volume, L small compared with I_c, we obtain $C_{K_{eff}(L)} = C_k(r=0)$ as it should. In the opposite case, considering large upscaling volumes L provides

$$C_{K_{eff}(L)} \simeq C_k(r=0)\left(\sqrt{2\pi}\frac{I_c}{L}\right)^D$$

This is a form of a central limit theorem for effective conductivity, quantifying the variance reduction leading to convergence of the effective conductivity for large averaging volume.

Finally, using the simplified expression (C.5), one gets after integration:

$$C_{K_{eff}}(L) \simeq C_k(r=0)\left[\sqrt{2\pi}\frac{I_c}{L}\,\mathrm{erf}\left(2\sqrt{2}\frac{L}{I_c}\right)\right]^D \tag{C.9}$$

It shares the same asymptotic behavior for extreme L than the exact (13). The same calculations can be carried out for $C_{\log K_{eff}}(L)$ and give the same results using $C_{\log k}(r=0)$) and the same spatial dependance.

Appendix D. Second order evaluation of the average of block K_{diss}

The block equivalent conductivity $K_{diss}(\vartheta)$ is given by Eq. (15). Decomposing the conductivity as $k(\mathbf{r}) = \langle k\rangle + \delta k(\mathbf{r})$, one can carry-out a second order expansion of $K_{diss}(\vartheta)$:

$$K_{diss}(\vartheta) = \frac{\int_\vartheta d^D\mathbf{r}(\langle k\rangle+\delta k)(\nabla(p_0+\delta p)^2}{\lambda^D\overline{\nabla(p_0+\delta p)}^2}.$$

This formula must be expanded up to second order in a series expansion of δk. Note that the technique that was presented in Appendix B cannot be followed directly because the variational formulation is efficient at the scale of the whole Ω only, not on every subvolume ϑ. In order to simplify notations, we introduce $\delta p(\mathbf{r})$ as the first order variation due to a variation $\delta k(\mathbf{r})$. The numerator can be expanded up to second order, discarding third order terms to yield:

$$\int_\vartheta d^D\mathbf{r}\,(\langle k\rangle+\delta k)\big(\nabla(p_0+\delta p)\big)^2 \simeq \int_\vartheta d^D\mathbf{r}(\langle k\rangle+\delta k)(1+2\nabla p_0\cdot\nabla\delta p) + \int_\vartheta d^D\mathbf{r}\langle k\rangle(\nabla\delta p)^2. \tag{D.1}$$

An analogous calculation can be carried out for the denominator, recalling that $\nabla p_0(\mathbf{r}') = \mathbf{e_x}$:

$$\begin{aligned} \lambda^D\overline{\nabla(p_0+\delta p)}^2 &= \lambda^D\left(\overline{\nabla(p_0)}^2 + 2\overline{\nabla p_0}\cdot\overline{\nabla\delta p} + \overline{\nabla\delta p}^2\right) \\ &= \lambda^D\left(1 + 2\overline{\nabla p_0}\cdot\overline{\nabla\delta p} + \overline{\nabla\delta p}^2\right) \end{aligned} \tag{D.2}$$

Combining Eq. (D.1) and the second order expansion of Eq. (D.2), many cancellations occur, yielding still at same order of approximation:

$$\begin{aligned} K_{diss}(\vartheta) = \overline{k} + \frac{1}{\lambda^D}\Big[&2\int_\vartheta d^D\mathbf{r}\,\delta k\left(\nabla p_0\cdot\nabla\delta p - \overline{\nabla p_0}\cdot\overline{\nabla\delta p}\right) \\ &+\langle k\rangle\int_\vartheta d^D\mathbf{r}\,((\nabla\delta p)^2 - \overline{\nabla\delta p}^2)\Big] \end{aligned}$$

One has in the general case $\overline{\nabla p_0} = \nabla p_0 = \mathbf{e}_x$. It can be observed that in the case of small averaging volume ϑ, $K_{diss}(\vartheta) = k(\mathbf{r})$ as it should: all the contributions cancel each other, because in that limit a volume average is equal to the local value: $\overline{\nabla\delta p} = \nabla\delta p$. Further simplifications can be obtained using Green's formula on the term $\langle k\rangle\int_\vartheta d^D\mathbf{r}(\nabla\delta p)^2$ combined with Eq. (A.1) that drives δp, yielding:

$$\begin{aligned} K_{diss}(\vartheta) = \overline{k} &+ \frac{1}{\lambda^D}\int_\vartheta d^D\mathbf{r}\,\delta k\,\nabla p_0\cdot\nabla\delta p \\ &- \frac{1}{\lambda^D}\left(2\int_\vartheta d^D\mathbf{r}\,\delta k\overline{\nabla p_0}\cdot\overline{\nabla\delta p} + \int_\vartheta d^D\mathbf{r}\langle k\rangle\overline{\nabla\delta p}^2\right) \\ &+ \frac{\langle k\rangle}{\lambda^D}\int_{\partial\vartheta} d^{D-1}\mathbf{r}\,\delta p\,\nabla\delta p\cdot\mathbf{n} + \frac{1}{\lambda^D}\int_{\partial\vartheta} d^{D-1}\mathbf{r}\,\delta k\,\delta p\,\nabla p_0\cdot\mathbf{n}. \end{aligned} \tag{D.3}$$

We obtain after statistical averaging:

$$\begin{aligned} \langle K_{diss}(\vartheta)\rangle = \langle k\rangle &- \frac{1}{\lambda^D}\int_\vartheta d^D\mathbf{r}\int_\Omega d^D\mathbf{r}'\,\nabla p_0(\mathbf{r}).\nabla\frac{\delta p(\mathbf{r})}{\delta k(\mathbf{r}')}\,C(\mathbf{r}'-\mathbf{r}) \\ &- \frac{1}{\lambda^D}\int_\vartheta d^D\mathbf{r}\left(2\langle\delta k\,\overline{\nabla p_0}\cdot\overline{\nabla\delta p}\rangle + \langle k\rangle\langle\overline{\nabla\delta p}^2\rangle\right) \\ &+ \frac{\langle k\rangle}{\lambda^D}\int_{\partial\vartheta} d^{D-1}\mathbf{r}\langle\delta p\,\nabla\delta p\cdot\mathbf{n}\rangle + \frac{1}{\lambda^D}\int_{\partial\vartheta} d^{D-1}\mathbf{r}\langle\delta k\,\delta p\rangle\nabla p_0\cdot\mathbf{n}. \end{aligned}$$

Using

$$\frac{\delta p(\mathbf{r})}{\delta k(\mathbf{r}')} = \frac{1}{\langle k\rangle}\nabla\cdot[G(\mathbf{r},\mathbf{r}')\nabla p_0(\mathbf{r}')],$$

and combining this result with Eq. (D.2), one obtains:

$$\begin{aligned} \langle K_{diss}(\vartheta)\rangle = \langle k\rangle &- \frac{1}{\langle k\rangle l^D}\int_\vartheta d^D\mathbf{r}\int_\Omega d^D\mathbf{r}'\partial_{r_x}\partial_{r'_x}G(\mathbf{r},\mathbf{r}')C_k(\mathbf{r}'-\mathbf{r}) \\ &- \frac{1}{\lambda^D}\int_\vartheta d^D\mathbf{r}(\langle 2\delta k\,\overline{\nabla p_0}\cdot\overline{\nabla\delta p}\rangle + \langle k\rangle\langle\overline{\nabla\delta p}^2\rangle) \\ &+ \frac{\langle k\rangle}{\lambda^D}\int_{\partial\vartheta} d^{D-1}\mathbf{r}\langle\delta p\,\nabla\delta p\cdot\mathbf{n}\rangle + \frac{1}{\lambda^D}\int_{\partial\vartheta} d^{D-1}\mathbf{r}\langle\delta k\,\delta p\rangle\nabla p_0\cdot\mathbf{n}. \end{aligned} \tag{D.4}$$

It can be checked by direct inspection that first line of this formula compares well with Eq. (B.3). The other contributions are finite size effects that cancel if $\vartheta = \Omega$. They explain the observed differences in the numerical tests. If ϑ tends to zero, $\langle K_{diss}(\vartheta)\rangle = \langle k\rangle$.

Supplementary material

Supplementary material associated with this article can be found, in the online version, at doi:10.1016/j.advwatres.2020.103594.

References

Ababou, R., 1994. Solution of stochastic groundwater flow by infinite series, and convergence of the one-dimensional expansion. Stochastic Hydrol. Hydraul. 8 (2), 139–155.

Ababou, R., 1996. Random porous media flow on large 3-D grids: numerics, performance, and application to homogenization. In: Environmental Studies. Springer, pp. 1–25.

Ababou, R., McLaughlin, D., Gelhar, L.W., Tompson, A.F., 1989. Numerical simulation of three-dimensional saturated flow in randomly heterogeneous porous media. Transp. Porous Media 4 (6), 549–565.

Abramovich, B., Indelman, P., 1995. Effective permittivity of log-normal isotropic random media. J. Phys. A 28 (3), 693.

Aguilar-Madera, C.G., Herrera-Hernández, E.C., Espinosa-Paredes, G., 2019. Solute transport in heterogeneous reservoirs: upscaling from the Darcy to the reservoir scale. Adv. Water Resour. 124, 9–28.

Akber Hassan, W.A., Jiang, X., 2012. Upscaling and its application in numerical simulation of long-term CO2 storage. Greenhouse Gases 2 (6), 408–418.

Armstrong, S., Kuusi, T., Mourrat, J.-C., 2019. Quantitative Stochastic Homogenization and Large-Scale Regularity, vol. 352. Springer.

Attinger, S., 2003. Generalized coarse graining procedures for flow in porous media. Comput. Geosci. 7 (4), 253–273.

Auriault, J., 1983. Effective macroscopic description for heat conduction in periodic composites. Int. J. Heat Mass Transf. 26 (6), 861–869.

Bauer, D., Talon, L., Ehrlacher, A., 2008. Computation of the equivalent macroscopic permeability tensor of discrete networks with heterogeneous segment length. J. Hydraul. Eng. 134 (6), 784–793.

Berkowitz, B., Balberg, I., 1993. Percolation theory and its application to groundwater hydrology. Water Resour. Res. 29 (4), 775–794.

Bernabé, Y., Li, M., Tang, Y.-B., Evans, B., 2016. Pore space connectivity and the transport properties of rocks. Oil Gas Sci. Technol. 71 (4), 50.

Bernabé, Y., Mok, U., Evans, B., Herrmann, F., 2004. Permeability and storativity of binary mixtures of high- and low-permeability materials. J. Geophys. Res. 109 (B12).

Beucher, H., Renard, D., 2016. Truncated gaussian and derived methods. C.R. Geosci. 348 (7), 510–519.

Bøe, Ø., 1994. Analysis of an upscaling method based on conservation of dissipation. Transp. Porous Media 17 (1), 77–86.

Boschan, A., Noetinger, B., 2012. Scale dependence of effective hydraulic conductivity distributions in 3D heterogeneous media: a numerical study. Transp. Porous Media 94 (1), 101–121.

Bruggeman, V.D., 1935. Berechnung verschiedener physikalischer konstanten von heterogenen substanzen. I. Dielektrizitätskonstanten und leitfähigkeiten der mischkörper aus isotropen substanzen. Ann. Phys. 416 (7), 636–664.

Celia, M.A., Bachu, S., Nordbotten, J., Bandilla, K., 2015. Status of CO2 storage in deep saline aquifers with emphasis on modeling approaches and practical simulations. Water Resour. Res. 51 (9), 6846–6892.

Chen, Y., Durlofsky, L.J., Gerritsen, M., Wen, X.-H., 2003. A coupled local–global upscaling approach for simulating flow in highly heterogeneous formations. Adv. Water Resour. 26 (10), 1041–1060.

Dagan, G., 1989. Flow and Transport in Porous Formations. Springer-Verlag GmbH & Co. KG..

Dagan, G., 1993. Higher-order correction of effective permeability of heterogeneous isotropic formations of lognormal conductivity distribution. Transp. Porous Media 12 (3), 279–290.

Dagan, G., Fiori, A., Jankovic, I., 2013. Upscaling of flow in heterogeneous porous formations: Critical examination and issues of principle. Advances in Water Resources 51, 67–85. 35th Year Anniversary Issue

Davit, Y., Quintard, M., 2017. Technical notes on volume averaging in porous media i: how to choose a spatial averaging operator for periodic and quasiperiodic structures. Transp. Porous Media 119 (3), 555–584.

De Wit, A., 1995. Correlation structure dependence of the effective permeability of heterogeneous porous media. Phys. Fluids 7 (11), 2553–2562.

Desbarats, A., 1992. Spatial averaging of hydraulic conductivity in three-dimensional heterogeneous porous media. Math. Geol. 24 (3), 249–267.

Desbarats, A., Srivastava, R., 1991. Geostatistical characterization of groundwater flow parameters in a simulated aquifer. Water Resour. Res. 27 (5), 687–698.

Durlofsky, L., 1998. Coarse scale models of two phase flow in heterogeneous reservoirs: volume averaged equations and their relationship to existing upscaling techniques. Comput. Geosci. 2, 73–92.

Durlofsky, L.J., 1991. Numerical calculation of equivalent grid block permeability tensors for heterogeneous porous media. Water Resour. Res. 27 (5), 699–708.

Durlofsky, L.J., 1992. Representation of grid block permeability in coarse scale models of randomly heterogeneous porous media. Water Resour. Res. 28 (7), 1791–1800.

Eberhard, J., Attinger, S., Wittum, G., 2004. Coarse graining for upscaling of flow in heterogeneous porous media. Multiscale Model. Simul. 2 (2), 269–301.

Gelhar, L.W., 1993. Stochastic Subsurface Hydrology. Prentice-Hall.

Godoy, V.A., Zuquette, L.V., Gómez-Hernández, J.J., 2018. Stochastic analysis of three-dimensional hydraulic conductivity upscaling in a heterogeneous tropical soil. Comput. Geotech. 100, 174–187.

Gray, W.G., Miller, C.T., 2005. Thermodynamically constrained averaging theory approach for modeling flow and transport phenomena in porous medium systems: 1. motivation and overview. Adv. Water Resour. 28 (2), 161–180.

Guadagnini, A., Riva, M., Neuman, S.P., 2018. Recent advances in scalable non-Gaussian geostatistics: the generalized sub-gaussian model. J. Hydrol..

Guin, A., Ritzi Jr., R.W., 2008. Studying the effect of correlation and finite-domain size on spatial continuity of permeable sediments. Geophys. Res. Lett. 35 (10).

Harbaugh, A.W., 2005. MODFLOW-2005, The US Geological Survey Modular Ground-Water Model: The Ground-Water Flow Process. US Department of the Interior, US Geological Survey Reston, VA.

Hashin, Z., Shtrikman, S., 1962. A variational approach to the theory of the effective magnetic permeability of multiphase materials. J. Appl. Phys. 33 (10), 3125–3131.

Hashin, Z., Shtrikman, S., 1963. A variational approach to the theory of the elastic behaviour of multiphase materials. J. Mech. Phys. Solids 11 (2), 127–140.

Hassanizadeh, M., Gray, W.G., 1979. General conservation equations for multi-phase systems: 1. Averaging procedure. Adv. Water Resour. 2, 131–144.

Hristopulos, D.T., 2020. Random Fields for Spatial Data Modeling A Primer for Scientists and Engineers. Springer.

Hunt, A., Ewing, R., Ghanbarian, B., 2014. Percolation Theory for Flow in Porous Media, vol. 880. Springer.

Hunt, A., Sahimi, M., 2017. Transport and reaction in porous media: percolation scaling, critical-path analysis, and effective-medium approximation. Rev. Geophys. 55.

Indelman, P., Abramovich, B., 1994. A higher-order approximation to effective conductivity in media of anisotropic random structure. Water Resour. Res. 30 (6), 1857–1864.

Indelman, P., Dagan, G., 1993. Upscaling of conductivity of heterogeneous formations: general approach and application to isotropic media. Transp. Porous Media. 12 (2), 161–183.

Indelman, P., Dagan, G., 1993. Upscaling of permeability of anisotropic heterogeneous formations: 2. General structure and small perturbation analysis. Water Resour. Res. 29 (4), 925–933.

Jacquard, P., 1965. Permeability distribution from field pressure data. Soc. Pet. Eng. J. 5 (4), 281–294.

Jikov, V.V., Kozlov, S.M., Oleinik, O.A., 2012. Homogenization of Differential Operators and Integral Functionals. Springer Science & Business Media.

Journel, A., Deutsch, C., Desbarats, A., et al., 1986. Power averaging for block effective permeability. SPE California Regional Meeting. Society of Petroleum Engineers.

Karimi-Fard, M., Durlofsky, L., 2016. A general gridding, discretization, and coarsening methodology for modeling flow in porous formations with discrete geological features. Adv. Water Resour. 96, 354–372.

King, P., 1989. The use of renormalization for calculating effective permeability. Transp. Porous Media 4 (1), 37–58.

Knudby, C., Carrera, J., 2005. On the relationship between indicators of geostatistical, flow and transport connectivity. Adv Water Resour 28 (4), 405–421.

Landau, L., Lifshitz, E., 1960. Electrodynamics of Continuous Media, vol. 8.

Le Loc'H, G., 1987. Etude de la composition des perméabilités par des méthodes variationnelles. Thèse de doctorat dirigée par Matheron, Georges Terre, océan, espace Paris, ENMP 1987 Ph.D. thesis.

Le Ravalec, M., Noetinger, B., Hu, L.Y., 2000. The FFT moving average (FFT-MA) generator: an efficient numerical method for generating and conditioning gaussian simulations. Math. Geol. 32 (6), 701–723.

Leung, J.Y., Srinivasan, S., 2012. Scale-up of mass transfer and recovery performance in heterogeneous reservoirs. J. Pet. Sci. Eng. 86–87, 71–86.

Liao, Q., Lei, G., Zhang, D., Patil, S., 2019. Analytical solution for upscaling hydraulic conductivity in anisotropic heterogeneous formations. Adv. Water Resour. 128, 97–116.

Linde, N., Renard, P., Mukerji, T., Caers, J., 2015. Geological realism in hydrogeological and geophysical inverse modeling: a review. Adv. Water Resour. 86.

Liu, Z.-F., Wang, X.-H., 2013. Finite analytic numerical method for two-dimensional fluid flow in heterogeneous porous media. J. Comput. Phys. 235, 286–301.

Malinouskaya, I., Preux, C., Guy, N., Etienne, G., 2018. Impact of geomechanical effects during SAGD process in a meander belt. Oil Gas Sci. Technol. 73, 17.

Masihi, M., Gago, P., King, P., 2016. Estimation of the effective permeability of heterogeneous porous media by using percolation concepts. Transp. Porous Media 114.

Matheron, G., 1967. Eléments pour une théorie des milieux poreux. Masson.

Maxwell, J.C., 1873. A Treatise on Electricity and Magnetism, vol. 1. Oxford: Clarendon Press.

Neuman, S.P., Orr, S., 1993. Prediction of steady state flow in nonuniform geologic media by conditional moments: exact nonlocal formalism, effective conductivities, and weak approximation. Water Resour. Res. 29 (2), 341–364.

Noetinger, B., 1994. The effective permeability of a heterogeneous porous medium. Transp. Porous Media 15, 99–127.

Noetinger, B., 2000. Computing the effective permeability of log-normal permeability fields using renormalization methods. Comptes Rendus de l'Académie des Sciences-Series IIA 331 (5), 353–357.

Noetinger, B., 2013. An explicit formula for computing the sensitivity of the effective conductivity of heterogeneous composite materials to local inclusion transport properties and geometry. Multiscale Model. Simul. 11 (3), 907–924.

Noetinger, B., Gautier, Y., 1998. Use of the Fourier-Laplace transform and of diagrammatical methods to interpret pumping tests in heterogeneous reservoirs. Adv. Water Resour. 21 (7), 581–590.

Noetinger, B., Zargar, G., 2004. Multiscale description and upscaling of fluid flow in subsurface reservoirs. Oil Gas Sci. Technol. 59 (2), 119–139.

Panzeri, M., Riva, M., Guadagnini, A., Neuman, S.P., 2016. Theory and generation of conditional, scalable sub-gaussian random fields. Water Resour Res. 52 (3), 1746–1761.

Pardo-Igúzquiza, E., Dowd, P.A., 2003. CONNEC3D: a computer program for connectivity analysis of 3D random set models. Comput. Geosci. 29 (6), 775–785.

Pozdniakov, S., Tsang, C.-F., 2004. A self-consistent approach for calculating the effective hydraulic conductivity of a binary, heterogeneous medium. Water Resour Res. 40 (5).

Preux, C., 2016. About the use of quality indicators to reduce information loss when performing upscaling. Oil Gas Sci. Technol. 71 (1), 7.

Quintard, M., Whitaker, S., 1998. Transport in chemically and mechanically heterogeneous porous media III. Large-scale mechanical equilibrium and the regional form of Darcy's law. Adv Water Resour 21 (7), 617–629.

Renard, P., De Marsily, G., 1997. Calculating equivalent permeability: a review. Adv. Water Resour. 20 (5), 253–278.

Riva, M., Guadagnini, A., Neuman, S.P., 2017. Theoretical analysis of non-gaussian heterogeneity effects on subsurface flow and transport. Water Resour. Res. 53 (4), 2998–3012.

Romeu, R., Noetinger, B., 1995. Calculation of internodal transmissivities in finite difference models of flow in heterogeneous porous media. Water Resour. Res. 31 (4), 943–959.
Rubin, Y., Gómez-Hernández, J.J., 1990. A stochastic approach to the problem of upscaling of conductivity in disordered media: theory and unconditional numerical simulations. Water Resour. Res. 26 (4), 691–701.
Sánchez-Vila, X., Girardi, J.P., Carrera, J., 1995. A synthesis of approaches to upscaling of hydraulic conductivities. Water Resour. Res. 31 (4), 867–882.
Sanchez-Vila, X., Guadagnini, A., Carrera, J., 2006. Representative hydraulic conductivities in saturated groundwater flow. Rev. Geophys. 44 (3).
Stauffer, D., Aharony, A., 2014. Introduction to Percolation Theory: Revised Second Edition. CRC press.
Stepanyants, Y.A., Teodorovich, E., 2003. Effective hydraulic conductivity of a randomly heterogeneous porous medium. Water Resour. Res. 39 (3).
Vereecken, H., Kasteel, R., Vanderborght, J., Harter, T., 2007. Upscaling hydraulic properties and soil water flow processes in heterogeneous soils a review. Vadose Zone J. 6, 1–28.
Wang, G.-W., Liu, Z.-F., Wang, X.-H., 2018. Finite analytic method for 2D steady fluid flows in heterogeneous porous media with unstructured grids. Int. J. Numer. Methods Eng. 113 (4), 742–766.
Wang, Y.-F., Liu, Z.-F., Wang, X.-H., 2014. Finite analytic numerical method for three-dimensional fluid flow in heterogeneous porous media. J. Comput. Phys. 278, 169–181.
Wen, X., Durlofsky, L., Edwards, M., 2003. Use of border regions for improved permeability upscaling. Math. Geol. 35 (5), 521–547.
Wen, X.-H., Gómez-Hernández, J.J., 1996. Upscaling hydraulic conductivities in heterogeneous media: an overview. J. Hydrol. 183 (1–2), 9–32.
Whitaker, S., 2013. The Method of Volume Averaging, vol. 13. Springer Science & Business Media.
Willot, F., Jeulin, D., 2009. Elastic behavior of composites containing boolean random sets of inhomogeneities. Int. J. Eng. Sci. 47 (2), 313–324.
Wood, B.D., Valdés-Parada, F.J., 2013. Volume averaging: Local and non local closures using a Green's function approach. Advances in Water Resources 51, 139–167. 35th Year Anniversary Issue
Wu, B., Liu, Z.-F., Wang, X.-H., 2013. Statistical behaviors for renormalization of correlated permeability field. Physica A 392 (15), 3115–3121.
Zheng, X.-L., Liu, Z.-F., Wang, X.-H., Shi, A.-F., 2017. Calculating the internodal transmissibilities using finite analytic method and its application for multi-phase flow in heterogeneous porous media. Int. J. Numer. Anal. Methods Geomech. 41 (1), 79–92.
Zhou, X.-Y., Gosling, P., Pearce, C., Kaczmarczyk, L., Ullah, Z., 2016. Perturbation-based stochastic multi-scale computational homogenization method for the determination of the effective properties of composite materials with random properties. Comput. Methods Appl. Mech. Eng. 300, 84–105.